Cold-set, crosslinker-free wood adhesives: A comparative study of ultrasound-extracted duck feather keratin and traditional food proteins

Nidal del Valle Raydan, Katharina Richter, Bertrand Charrier, Andreas Hartwig, Eduardo Robles

▶ **To cite this version:**

Nidal del Valle Raydan, Katharina Richter, Bertrand Charrier, Andreas Hartwig, Eduardo Robles. Cold-set, crosslinker-free wood adhesives: A comparative study of ultrasound-extracted duck feather keratin and traditional food proteins. Materials Today Sustainability, 2024, 27, 10.1016/j.mtsust.2024.100905 . hal-04672410

HAL Id: hal-04672410
https://univ-pau.hal.science/hal-04672410v1

Submitted on 19 Aug 2024

HAL is a multi-disciplinary open access archive for the deposit and dissemination of scientific research documents, whether they are published or not. The documents may come from teaching and research institutions in France or abroad, or from public or private research centers.

L'archive ouverte pluridisciplinaire **HAL**, est destinée au dépôt et à la diffusion de documents scientifiques de niveau recherche, publiés ou non, émanant des établissements d'enseignement et de recherche français ou étrangers, des laboratoires publics ou privés.

Materials Today Sustainability 27 (2024) 100905

Contents lists available at ScienceDirect

Materials Today Sustainability

journal homepage: www.journals.elsevier.com/materials-today-sustainability

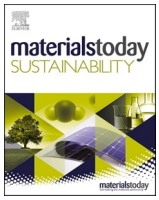

Cold-set, crosslinker-free wood adhesives: A comparative study of ultrasound-extracted duck feather keratin and traditional food proteins

Nidal Del Valle Raydan [a], Katharina Richter [b], Bertrand Charrier [a], Andreas Hartwig [b,c], Eduardo Robles [a,*]

[a] University of Pau and the Adour Region, E2S UPPA, CNRS, IPREM, Mont de Marsan, France
[b] Fraunhofer Institute for Manufacturing Technology and Advanced Materials IFAM, Bremen, Germany
[c] University of Bremen, Department 2 Biology/Chemistry, Bremen, Germany

ARTICLE INFO

Keywords:
Keratin
Biobased adhesives
Cold-set bonding
Crosslinker-free adhesives

ABSTRACT

This study investigates the potential of keratin, a waste from duck feathers, as a sustainable alternative for wood adhesive applications. Keratin was extracted by sonochemical hydrolysis, a green and innovative method. Keratin was compared in its properties with casein, soybean, and pea proteins, three of the most studied proteins, as alternative eco-friendly materials to petroleum-derived products. However, these proteins remain used in the food industry. Protein-based adhesives were activated with sodium and calcium hydroxide. A comprehensive analysis was also conducted to study the influence of solid content, alkali, pH, viscosity, polarity, and structural composition of adhesives on their mechanical properties. The thermal properties of proteins and adhesives and the effects of post-alkaline treatment on protein secondary structure, crosslinking, and water resistance were studied. The key finding is that keratin shows potential as an eco-friendly adhesive, with tensile shear strength tests on beech wood meeting European standards. In addition, it showed superior water resistance due to its effective crosslinking ability compared to other food-derived proteins. The results position keratin as a feasible replacement for food-derived and formaldehyde-based adhesives, offering a sustainable option for interior wood applications and presenting an environmentally friendly solution with appropriate performance.

1. Introduction

Developing environmentally friendly wood adhesives made with natural and renewable resources has attracted scientists and industrial actors in recent years. However, because of the performance of these bio-sourced adhesives both in terms of bond strength and water resistance, formaldehyde remains an integral part of these bio-based adhesive formulations to perform as well as synthetic formulations such as phenol-formaldehyde (PF) [1,2], urea-formaldehyde (UF) [3], and melamine urea formaldehyde (MUF) [4,5]. This is a major problem in terms of environmental impacts; first of all, formaldehyde is a petroleum-based material, which is a non-sustainable product [6], and secondly, while modern technologies have advanced to reduce formaldehyde emissions in wood products, achieving near-zero emissions in some instances, concerns still exist regarding emissions during production and over the product's life cycle [7]. As a result, legislation regarding the indoor environment and final product emissions has become increasingly strict, intending to achieve a zero-emission limit [8,9]. As such, future adhesives for wood should be completely formaldehyde-free. Nowadays, one of the popular techniques used to eliminate formaldehyde components is incorporating crosslinkers into bio-based formulations; however, some can be just as harmful as formaldehyde [10–12]. A promising environmentally friendly alternative is to use naturally occurring biopolymers such as proteins. The abundance of different types of protein as a waste product, whether from animals or plants, has made such materials attractive. Literature on using proteins in wood adhesives is extensive, and adequate reviews are available [13–15]. Most recent research has focused on the addition of co-reacting compounds to proteins, such as phenolics [16,17], polyamidoamine-epichlorohydrin [18,19], isocyanates, and epoxies [20–23], but other research has used aldehydes or added reactive functionality to the protein [24,25]. Some well-documented industrial processes use casein for wood adhesives, but they have never reached industrial application due to the low protein fraction compared to other higher protein sources, making them more expensive [26]. In the last ten years, soy-based adhesives have also been the subject of considerable

* Corresponding author.
E-mail address: eduardo.robles@univ-pau.fr (E. Robles).

https://doi.org/10.1016/j.mtsust.2024.100905
Received 26 March 2024; Received in revised form 15 June 2024; Accepted 4 July 2024
Available online 10 July 2024
2589-2347/© 2024 The Author(s). Published by Elsevier Ltd. This is an open access article under the CC BY license (http://creativecommons.org/licenses/by/4.0/).

research and have attracted attention due to their performance. Despite this, their use remains subject to critical issues. For instance, soy crops are not grown worldwide [27], and therefore, it is interesting to evaluate whether other waste proteins can perform similarly to casein or soy. Leguminous peas are among the other proteins readily available worldwide, and they have an amino acid profile similar to soybeans [28], so they can be used as an adhesive in principle. They usually have a steady annual growth rate; however, various factors can lead to price spikes and volatility for dry peas, lentils, and chickpeas. These include a decline in production driven by weather-reduced yields, lower global supplies, reduced domestic area as producers transition to high-priced competing crops such as wheat, soybeans, and corn, and global supply chain impacts from the Ukraine-Russia conflict [28]. Aside from the fact that these proteins may have many limitations, they also contribute significantly to industrial food and feed production. Demand for plant-based meat alternatives has increased, and more people are seeking alternatives to meat for health and sustainability reasons. Increasing consumer demand for meat-like products (meat analogs, as they are called in the industry) has triggered an innovation boom in the food science industry that, according to analysts, will more than double by 2030 [29]. Exploring new protein sources that do not compete with the food industry is proliferating in this context. One source is the keratinous wastes (feathers, skin, hair, wool, horns, among others) that are abundant worldwide [30]. Several challenges need to be addressed, such as understanding the concept of protein adhesives based on available feedstock without expensive solvents or processes that expose their reactive functional groups to wood (see Fig. 13).

A second issue for wood-based composite panels concerns the hot-press time required to produce them if thermoset adhesives are used, where the energy consumed during heating is the critical technical parameter determining the cost and profitability of both process and product. Therefore, developing adhesives that can be cured at room temperature is essential. Adhesives of this type are usually referred to as cold-set adhesives. Common cold-set adhesives include formaldehyde [24,31], polyurethanes–isocyanate-based adhesives– and other toxic combinations such as bisphenol A [32]. The development of an isocyanate-free and formaldehyde-free cold-set wood adhesive is desirable.

Furthermore, with modern safety standards becoming stricter worldwide, adhesives' thermal stability and flame-retardant properties have become more critical [33]. Protein-based adhesives show promise in addressing these concerns due to their ability to form a protective char, thereby reducing the risks associated with the emission of volatile organic compounds (VOCs) and formaldehyde, common issues with solvent, petroleum-based adhesives, and epoxy resins upon combustion [34]. Another challenge for protein-based adhesives is meeting the demands of current wood adhesive applications. One of these requirements is the balance between solid content and viscosity, which is crucial to obtaining high bond strength and spreadability [35]. Protein-based adhesives typically have low solid content due to viscosity constraints, so high water content poses an important challenge to producing wood composite materials, including particleboards and fiberboards [36]. Ideally, protein-based adhesives should contain a high solid content while minimizing their viscosity and improving their ability to penetrate the wood. In general, alkaline treatment of proteins is thought to enhance adhesive properties by exposing specific functional groups through unfolding, resulting in an increase in intermolecular interactions with the solvent/medium and a reduction in viscosity [37]. Several alkalis have been used previously for hydrolyzing proteins, including NaOH, $Ca(OH)_2$, $B_4Na_2O_7{\cdot}10H_2O$, Na_2HPO_4, and NH_4OH, showing that proper solvent choice affects protein solubility [38].

This study compared four proteins with similar isoelectric points, keratin, casein, soybean, and pea, for their adhesive properties to examine other alternatives to formaldehyde as wood adhesives for indoor applications. To such purpose, the dissolution of the proteins in two different alkalis, NaOH and $Ca(OH)_2$, was preliminarily considered to investigate further the effect of two different cations with different charges. Although most of the works mainly focused on developing adhesive systems with sufficient bonding strength by incorporating hazardous additives and crosslinkers, the relation between mechanical properties and the solid content of adhesive has not been sufficiently studied. The selected different proteins were alkaline treated at room temperature, and the effect of solid content, alkali, pH, subunit composition, viscosity, polarity, and decomposition profile were also investigated. The four different proteins, as well as raw duck feathers, were analyzed by attenuated total reflection infrared spectroscopy (ATR-IR), Raman spectroscopy (RS), Sodium Dodecyl Sulfate Poly-Acrylamide Gel Electrophoresis (SDS-PAGE), differential scanning calorimetry (DSC), thermogravimetric analysis (TGA), Matrix Assisted Laser Desorption Ionization-Time of Flight (MALDI-ToF), and Micro-scale combustion calorimetry (MCC). The alkaline-treated proteins were analyzed by Raman Spectroscopy (RS) and MCC. Changes in the cure state and viscosity of dispersions were monitored by Shear Viscometer (SV) and Dielectric Analysis (DEA), indicating protein structure alteration. Tensile shear strength measurements were performed on beech wood substrates bonded with the different protein formulations to investigate bond strength in dry conditions. Different ratios of (protein: water: alkali) influenced the shear strength values of the proteins differently. This work aims to better understand the bonding mechanism by correlating the mechanical properties of the different proteins to their structures, subunit composition, viscosity, solid content, alkali, and pH.

2. Materials and methods

2.1. Materials

Casein (CAS number: 9000-71-9) from bovine milk was supplied by Sigma Aldrich Chemie GmbH (Steinheim, Germany), and hydrolyzed pea protein (CAS number: 222400-29-5) and soy protein isolate (CAS number: 9010-10-0) were supplied by Sports Supplements Ltd. (Bulk Powders). Mulard duck feathers were provided cleaned and dried by Plum'Export (Saint-Sever, France). NaOH (CAS number 1310-73-2) was purchased from VWR Chemicals BDH® (Belgium), and Ca(OH)2 (CAS number: 1305-62-0) was purchased from Honeywell (Darmstadt, Germany).

2.2. Ultrasound-assisted alkaline hydrolysis of raw duck feather

The cleaned feathers were ground to 5 mm using an electric grain grinder (VEVOR, Windach, Germany) and then dissolved in a ratio of 10:100 in an aqueous solution of 3 % wt NaOH using a 26 kHz ultrasonic homogenizer (UP200St, Hielscher, Germany) with a maximal nominal power of 200 W, inside a beaker. A homogeneous colloid was obtained after 25 min with an average energy consumption of 0.045 kWh. Following this, the keratin colloid was filtered to remove the undissolved feather parts and then precipitated using oxalic acid to a pH of 4.5, followed by dialysis. The dialysis was performed against type II water over three days using a 6–8 kDa molecularporous membrane tubing (Spectra/Por®1, Spectrum Labs, USA). Neutralized samples were dried with a lyophilizer (Alpha 1–4, Martin Christ GmbH, Osterode am Harz, Germany). The weight of extracted keratin was compared to the total weight of feathers used in hydrolysis to calculate the relative yield (RY) as outlined in equation (1). The absolute yield (AY), detailed in equation (2), was determined by comparing the extracted keratin quantity against the initial keratin content in the feathers, which was determined through Kjeldahl's method at 83% of the total feather mass [39].

$$RY\ (\%) = [(M_0 - M_{dry})/M_0] \quad (1)$$

$$AY\ (\%) = [(0.83M_0 - M_{dry})/M_0] \quad (2)$$

M_0 is the initial quantity of feathers used for hydrolysis, M_{dry} is the

keratin hydrolysate lyophilized, and $0.83M_0$ is the consideration of 83% of the keratin content found in feathers.

2.3. Alkaline hydrolysis of proteins for adhesive development

Table 1 summarizes the dispersion compositions based on keratin, casein, soybean, and pea proteins used in this work. The dispersion nomenclature is also presented in Table 1. Calcium and sodium hydroxide were used as activating agents. The solids content was adjusted depending on the source of protein to obtain similar viscosity values. The adhesive formulations were prepared while stirring at room temperature, without heating, to avoid protein denaturation and energy consumption. pH measurements were conducted for all 40 formulations to ensure precision and consistency. A detailed flow diagram is included in the Supporting Information as Fig. S1 to represent the experimental process visually. The total dispersion volume was 8 mL.

3. Characterization

3.1. Attenuated total reflection infrared spectroscopy

Functional groups of ground feathers and different protein isolates were analyzed by Fourier Transform Infrared (FT-IR) spectroscopy with Attenuated Total Reflectance (ATR) mode with a Bruker ALPHA II series spectrometer combined with an ALPHA's Platinum ATR single reflection diamond ATR module. All spectra were recorded over a 4000-400 cm^{-1} frequency range using 64 scans and 2 cm^{-1} resolution.

3.2. Raman spectroscopy

RAM II module was employed to obtain the Raman spectra in the spectral range between 800 and 3600 cm^{-1} using a diode-pumped Nd: YAG laser with an excitation wavelength of 1064 nm at a laser power of 150 mW. Each spectrum had an average of 250 scans, replicated at least three times per analysis.

3.3. Electrophoresis analysis

The Sodium Dodecyl Sulfate PolyAcrylamide Gel Electrophoresis (SDS-PAGE) analysis was performed using the Laemmli method [40] for all four proteins and feathers. A bovine albumin standard (2 mg/mL) was used as a reference. All samples were incubated in 2x Laemmli buffer for 5 min at 95 °C to ensure denaturation. The buffer consisted of 250 mM Tris-HCl (pH 6.8), 8% SDS, 40% glycerol, 8% 2-mercaptoethanol, and 0.02% bromophenol blue.

For the gel preparation, 10 μL Prestained Protein Ladder (10–250 kDa, Thermo Scientific) was loaded in lane 1, while 10 μL of the different protein isolates and bovine albumin standard were loaded in separate wells of the subsequent lanes. The electrophoresis process utilized Bolt™ 4–12% Bis-Tris Plus Gel (Invitrogen™ NW04120BOX, USA) and SDS running buffer. The gels were run at 180 V until the dye front reached the bottom of the gel. Following electrophoresis, the gels were stained with Coomassie Brilliant blue R 250 and rinsed with 5% acetic acid and 20% methanol until a clear background was observed.

Table 1
Formulations of keratin, casein, soybean, and pea proteins with corresponding nomenclatures.

Alkali	Protein	Protein (g)	Water (g)	Alkali (g)	pH	Nomenclature
$Ca(OH)_2$	Keratin	1.5	8	0.2	12.37	K-1.5-Ca-0.2
		1.5	8	0.5	12.4	K-1.5-Ca-0.5
		3.5	8	0.2	12.06	K-3.5-Ca-0.2
		3.5	8	0.5	12.05	K-3.5-Ca-0.5
		4	8	0.2	11.21	K-4-Ca-0.2
		4	8	0.5	12.18	K-4-Ca-0.5
	Casein	1.5	8	0.2	12.84	C-1.5-Ca-0.2
		1.5	8	0.5	12.93	C-1.5-Ca-0.5
		2.5	8	0.2	11.97	C-2.5-Ca-0.2
		2.5	8	0.5	12.01	C-2.5-Ca-0.5
		3.5	8	0.2	11.35	C-3.5-Ca-0.2
		3.5	8	0.5	11.85	C-3.5-Ca-0.5
	Soybean	1.5	8	0.2	12.46	S-1.5-Ca-0.2
		1.5	8	0.5	12.35	S-1.5-Ca-0.5
		2	8	0.2	12.47	S-2-Ca-0.2
		2	8	0.5	12.51	S-2-Ca-0.5
	Pea	1.5	8	0.2	12.27	P-1.5-Ca-0.2
		1.5	8	0.5	12.34	P-1.5-Ca-0.5
		2	8	0.2	12.04	P-2-Ca-0.2
		2	8	0.5	12.19	P-2-Ca-0.5
NaOH	Keratin	1.5	8	0.2	13.14	K-1.5-Na-0.2
		1.5	8	0.5	13.65	K-1.5-Na-0.5
		3.5	8	0.2	12.65	K-3.5-Na-0.2
		3.5	8	0.5	13.12	K-3.5-Na-0.5
		4	8	0.2	11.9	K-4-Na-0.2
		4	8	0.5	13.45	K-4-Na-0.5
	Casein	1.5	8	0.2	12.99	C-1.5-Na-0.2
		1.5	8	0.5	13.55	C-1.5-Na-0.5
		2.5	8	0.2	12.78	C-2.5-Na-0.2
		2.5	8	0.5	13.12	C-2.5-Na-0.5
		3.5	8	0.2	11.02	C-3.5-Na-0.2
		3.5	8	0.5	13.25	C-3.5-Na-0.5
	Soybean	1.5	8	0.2	13.18	S-1.5-Na-0.2
		1.5	8	0.5	13.47	S-1.5-Na-0.5
		2	8	0.2	12.99	S-2-Na-0.2
		2	8	0.5	13.19	S-2-Na-0.5
	Pea	1.5	8	0.2	12.89	P-1.5-Na-0.2
		1.5	8	0.5	13.13	P-1.5-Na-0.5
		2	8	0.2	12.65	P-2-Na-0.2
		2	8	0.5	13.24	P-2-Na-0.5

3.4. Matrix-assisted laser desorption/ionization-time of flight mass spectrometry

The different protein isolates were identified using matrix-assisted laser desorption/ionization-time of flight mass spectrometry (MALDI-ToF MS). Before mass spectrometry, samples were desalinated with washing steps (10 times). Samples were prepared using dried droplet preparation: HCCA (M = 164,16 g/mol) in a concentration of 20 mg/mL (m/v corresponds to 0.12 mmol) dissolved to saturation in a mixture of acetonitrile, water, and trifluoroacetic acid (70/30/0.1 resp., v/v/v). The matrix was mixed 10:1 (v/v) with the sample dissolved in 70 % acetonitrile. 1 μL of this solution was deposited on a brushed steel MALDI target (Bruker Daltonik, Bremen, Germany). After solvent evaporation, the MALDI-ToF-MS spectra were obtained using an Nd: YAG laser (355 nm) on an autoflex speed LRF MALDI MS with a MALDI-Perpetual ion source and BRUKER smartbeam-II laser (Bruker Daltonik, Bremen, Germany). In positive mode (linear and reflector mode), the signals of 500 laser shots at five different positions were accumulated. Different mass ranges were investigated. Peptide mass mapping was done using FlexAnalysis from Bruker (Version 3.4) mass spectrometer.

3.5. Viscosity measurements

Viscosity measurements were carried out on all formulations at ambient temperature (25 °C), with a rheometer (DVNext–RV, AMETEK Brookfield Inc., Élancourt, France), using a low-volume adapter (SC4-13R) and spindle (SC4-27) with a scale from 250,000 to 500,000 cP [41]. All data were taken after 1 min of spindle rotation. The rotational velocity was adjusted to 250 rpm for samples of low viscosity and 0.5 rpm for samples of high viscosity to reach a torque close to 90 %. Sixteen samples were too viscous to be analyzed with the SC4-27 spindle. The viscosity was calculated by multiplying the dial reading or % torque by the factor corresponding to the viscometer spindle and speed used. This was measured using complete computer control regarding the "Rheocalc" software, which collected data automatically.

3.6. Dielectric analysis

Dielectric analysis (DEA) was done using a dielectric analyzer (DEA 288 Ionic, NETZSCH Gerätebau GmbH), with single-use interdigitating sensors used to monitor the curing process of the thermoset adhesives at room temperature. For this purpose, the ion viscosity, increasing with the degree of curing, was measured at different frequencies (1, 10, and 100 Hz). The DEA measurements were evaluated with NETZSCH's Proteus® software.

3.7. Measurement of contact angle

The contact angle was measured using an optical tensiometer (Theta Flow, Biolin Scientific, Sweden/Finland) using the sessile drop method. For this, beech wood samples were coated with a 2 mm layer of the prepared adhesive. Only adhesive formulations (Protein 1.5g - Alkali 0.5g) were analyzed. The contact angles were measured on the surface of the dried adhesive coatings with water as the test liquid. The duration of each measurement was 10 s, and the measurement was repeated thrice. The drop shapes were fitted to the Young-Laplace equation.

3.8. Thermal analysis

3.8.1. Thermogravimetric analysis (TGA)

The thermal resistance of ground feathers and different protein isolates were measured with a thermogravimeter (TGA Q500, TA instruments, Guyancourt, France); samples were heated from 30 °C to 800 °C at 10 °C/min under a nitrogen atmosphere.

3.8.2. Differential scanning calorimetry

The melting temperatures of ground feathers and different protein isolates were measured using differential scanning calorimetry (DSC) on a calorimeter (Discovery DSC, TA Instruments, Eschborn, Germany) under a continuous nitrogen purge at a heating rate of 10 K/min over a temperature range from −50 °C to 250 °C. The samples were placed in standard aluminum pans with standard lids. The DSC cell was calibrated with indium (m.p. 156.6 °C; $\Delta H_m = 28.54$ J/g). An empty pan sealed with a cover pan was used as a reference sample. TRIOS software (TA Instruments) was used to identify the melting temperature. The melting temperature was determined by extrapolating the starting point (T onset) of the endothermic peak during heating; the intersection of the tangent with the point of maximum slope with the baseline was extrapolated.

3.8.3. Micro combustion calorimetry

Micro Combustion Calorimetry (MCC) was measured on a calorimeter (FTT FAA Micro Calorimeter, Fire Testing Technology Limited, United Kingdom) following ASTM D7309-07 Method A. Approximately 12 mg of each protein, as well as feathers and the adhesive formulations (Protein 1.5g - Alkali 0.5g), were separately heated in a pyrolysis chamber. The heating rate was 1 °C/s from 150 to 600 °C under a nitrogen flow of 80 mL/min. The volatile pyrolysis products entered the combustor and were combusted at 900 °C in a nitrogen/oxygen mix (80:20 mL/min). The temperature-dependent heat release of the combustion using oxygen consumption calorimetry was determined by measuring the oxygen concentration before and after the combustion. The resulting spectra were fitted using software from Fire Testing Technology.

3.9. Lap shear test strength

The modified protein solutions were used to join pieces of beech wood (Konrad Bruckeder, Rosenheim, Germany) pre-conditioned at 23 °C and 50 % relative humidity for 4 weeks for the adhesive strength evaluation. The prepared 40 protein formulations of 0.25 mL were applied with a brush onto a defined area of 2 cm^2 on the beech wood pieces. After application, a second wood piece was pressed on the adhesive area, lined up in rows of 10 samples each time, and cured with 65 bar pressure for 2 h. Afterwards, the samples were allowed to dry without pressure at room temperature for 12 h. Lap shear tests were performed with all samples to determine the shear strength exhibited by the adhered wood samples using a universal testing machine (UTS Testsysteme GmbH, Ulm, Germany). The substrate failures were observed with an AM7115MT-FUW microscope (Dino-Lite, Taiwan) at 50 magnifications.

3.10. Statistical analysis

Analysis of variance (ANOVA) and *t*-test calculations were used to test ($p < 0.05$) for significant differences between factors and levels using OriginPro 2023. The means were compared when the ANOVA indicated a significant difference using the Tukey test. Where applicable, the mean values of the investigated features and the standard deviation indicated as error bars have been presented on the plots.

3.11. Sol-gel test

The sol-gel tests were performed to investigate the degree of cross-linking of the different protein-based adhesives chosen, taking into consideration the best performance in the lap shear test and the similarity of alkali concentrations (K-4-Na-0.2; K-4-4-Ca-0.5; C-2.5-Na-0.2; C-2.5-Ca-0.5; S-2-Na-0.2; S-2-Ca-0.5; P-2-Na-0.2; P-2-Ca-0.5). The prepared adhesive was cured at 120 ± 3 °C and dried to a constant weight (M_1). Next, the samples were immersed in water for 6 h at 60 ± 3 °C and then dried at 105 ± 3 °C to obtain a stable mass (M_2). The gel content

(C_{gel}) was calculated using equation (3):

$$C_{gel}\ (\%) = [(M_2)/M_1] \times 100 \quad (3)$$

Three parallel tests were conducted for each sample, and the average value was reported.

3.12. Water uptake test

The water resistance properties of the protein-based adhesives chosen taking into consideration the best performance in the lap shear test and the similarity of alkali concentrations (K-4-Na-0.2; K-4-4-Ca-0.5; C-2.5-Na-0.2; C-2.5-Ca-0.5; S-2-Na-0.2; S-2-Ca-0.5; P-2-Na-0.2; P-2-Ca-0.5), were tested using a water uptake test. The adhesives were completely cured to a constant weight (M_3) at 120 ± 3 °C and then assessed by gravimetric analysis at a temperature of 50 ± 3 °C and a humidity of 80%. The weight of the sample was recorded every 2 h until it reached a stable value (M_4). The water uptake (WU) was calculated using equation (4):

$$WU\ (\%) = [(M_4 - M_3)/M_3] \times 100 \quad (4)$$

4. Results and discussion

4.1. Yield of keratin hydrolysate

The protein content in the raw duck feathers used in this study amounted to 82.97 ± 0.98%, as determined by Kjeldahl's method. The effect of ultrasound-alkaline-assisted hydrolysis of feathers on the yield of keratin resulted in a relative yield of 61.8 ± 5 % and an absolute yield of 74.5 ± 5%.

4.2. Fourier-transform infrared spectroscopy

Understanding protein-surface interactions is crucial for the design of bioadhesives. The ATR-IR spectra of unmodified proteins (Fig. 1) show general similarities with minor protein-specific variations. These spectra were normalized to the Amide I band at 1634 cm^{-1}. All proteins exhibit 5 characteristic bands, four of which are amide bands. The broad peak at 3300–3200 cm^{-1} is attributed to Amide A. This band comes from the stretching vibration of the NH bond, and its frequency depends on the strength of hydrogen bonds, which can also involve interactions with O–H groups [42]. The Amide I band, primarily influenced by C═O stretch and weakly with C–N stretch and N–H bending, is found between 1600 and 1700 cm^{-1}. The exact band position is determined by the backbone conformation and the hydrogen bonding pattern within the protein molecule [43]. The Amide II band, occurring at 1500–1600 cm^{-1}, is mainly derived from the C–N stretch and N–H in-plane bending. Lastly, at 1200–1300 cm^{-1}, the Amide III band represents a complex mix of N–H bending and C–N stretching along with C–H and N–H deformation vibrations [43–45]. These amide bands, especially Amide I, are crucial for determining the protein's secondary structure [46]. Analysis of the Amide I band was done through curve fitting using the second derivative to identify hidden bands and Gaussian curves to fit the curve until a coefficient of determination above 0.9995 was achieved. This reveals the presence and proportion of α-helix, β-sheets (intermolecular Antiparallel (inter. AP); intramolecular Parallel (intra. P); and turn/-random coil structures, β-sheets (inter. AP)/side chains in the Supplementary Information Fig. S3 and Table S1. In general, α-helical structures have a band at wavenumbers 1650–1658 cm^{-1}; β-sheet structures tend to have bands between 1620 and 1640 cm^{-1} and between 1670 and 1695 cm^{-1}; random coil structures occur at around 1644 cm^{-1} [46]. Clear differences in the resolved Amide I bands were observed. The analysis reveals a higher proportion of β-sheet (inter. AP) structures in all proteins, which also exhibit a lower α-helix content, given a ratio (β-sheet (inter. AP)/α-helix) of 0.31 for feathers, increasing to 1.3 for keratin, while Pea has 1.6, and Soybean and Casein 2.0. A higher β-sheet content contributes to higher solubility, which might contribute to keratin's lower protein solubility than other sources [47].

Additionally, ATR-IR spectra show the 3278 cm^{-1} band representing N–H stretching in secondary amides and amines. The 2930 cm^{-1} band corresponds to the $–CH_2$ group. Notably, the carbonyl ester band (1740 cm^{-1}), unique to pea protein, suggests differences in pre-treatment or hydrolysis compared to other proteins.

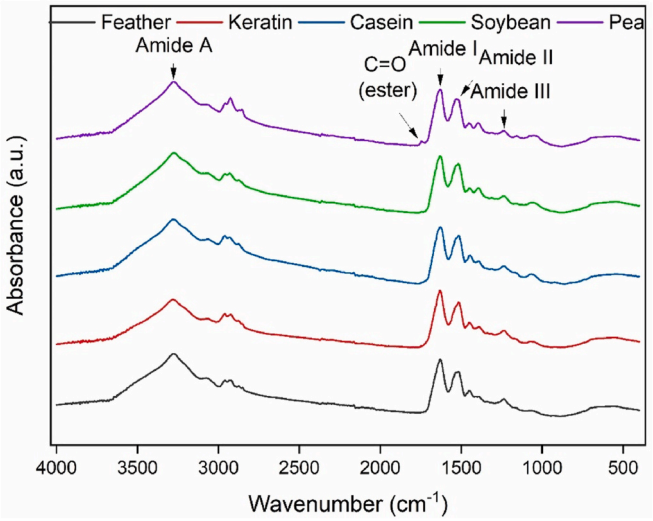

Fig. 1. ATR-IR spectra of feathers and proteins.

4.3. Raman spectroscopy

Raman spectroscopy has been highly influential in studying protein conformational changes, particularly in analyzing structural and functional shifts up to protein unfolding or denaturation [48]. Raman spectra of the -cystine and -cysteine are presented in Fig. 2a. Notably, peaks at 2552 cm^{-1}, 940 cm^{-1}, 870 cm^{-1}, 822 cm^{-1}, 774 cm^{-1}, and 537 cm^{-1} corresponded to the S–H group stretching frequency; these peaks were absent in -cystine's Raman spectrum. In comparison, a peak at 498 cm^{-1} appeared according to the -cysteine curve, which was associated with the S–S bond. The most outstanding peak, centered near ≈1670 cm^{-1} for all proteins Fig. 2b-e, has been assigned to the Amide I vibration mode, mainly involving the extension of C═O and C–N. The Amide III peaks (≈1204 cm^{-1}, ≈1250 cm^{-1}, ≈1278 cm^{-1}, ≈1311 cm^{-1}, and ≈1343 cm^{-1}) mainly involve the extension of C–N and the planar transition of NH [49]. The C–C stretching vibrations at 1239 cm^{-1}, characteristic of β-sheet structures, are also noted [50]. A marked increase in the intensity of this peak in keratin compared to raw duck feathers (Fig. 2b) confirms the ATR-IR results.

Stretching vibrations involving saturated and aromatic C–H bonds yield higher Raman intensities in keratin due to the abundance of such groups, compared to raw feathers, and decrease upon alkaline treatment due to unfolding. The vibrational modes at ≈150 cm^{-1} and ≈220 cm^{-1} represent asymmetric S–S bending and symmetric S–S bending, respectively [51], with the peak at 473 cm^{-1} and an associated shoulder at ≈467 cm^{-1} diverging from the typical S–S stretch found in cystine around ≈500 cm^{-1}. Disulfide bridges at 153 cm^{-1}, 220 cm^{-1}, and 473 cm^{-1} were not visible in raw feathers due to the complex native structure, whereas these appear in keratin, indicating disulfide bond cleavage and subsequent structural reorganization (Fig. 2b). Alkaline treatment can unfold protein structures, reducing peak intensities by disrupting hydrogen bonds and other intramolecular interactions, leading to a more open structure that scatters light differently [52]. In-plane vibrations of the rings of aromatic side chains (Trp, Tyr, Phe) in Fig. 2(b–e)

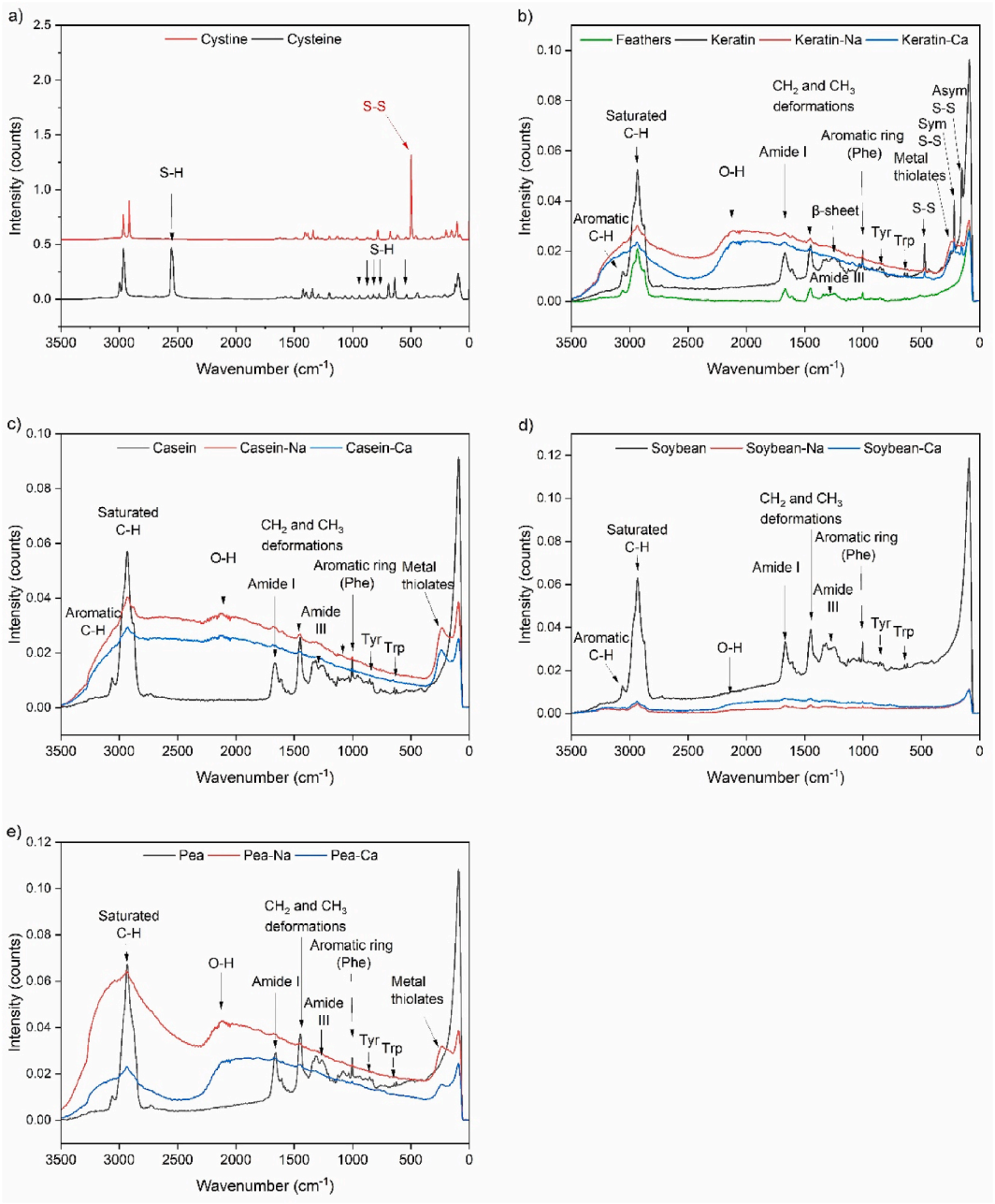

Fig. 2. Raman spectroscopy analysis of cystine, cysteine, feathers, untreated and alkaline treated proteins.

are lower after alkaline treatment due to denaturation [53]. New peaks in the keratin, casein, and pea proteins' spectra but not in the soybean protein (Fig. 2 b, c, and e) in the range of 230–240 cm^{-1} could be due to the formation of thiolates due to the presence of amino acids like cysteine and methionine, which contain thiol (-SH) or sulfide (S–S) groups [54]. The alkali treatments can lead to the deprotonation of thiol groups or breakage of disulfide bonds, which could form new compounds with sodium or calcium ions, resulting in metal thiolates $M(SR)_x$ [55]. These peaks can be somewhat higher in frequency for heavier metal thiolates than sodium in the case of calcium. Previous studies indicate that at pH 12.2 and ambient temperature, aggregation begins with disulfide bond breakage, destabilizing α-helix and –SH group in cysteines available for intermolecular bonding, increasing intramolecular distances and facilitating β-sheet formation in aggregated proteins. This was shown in the ATR-IR analysis of the Amide I band in keratin, showing a decrease in α-helix and an increase in β-sheets compared to feathers and aggregations in certain keratin adhesive formulations [56]. The 2400–2500 cm^{-1} peak could be associated with stretching OH-group vibrations (Fig. 2b-e), which may become more pronounced upon protein unfolding or interaction with alkali. Hence, theoretically, proteins treated with alkali have the potential to form more robust adhesives, as the treatment exposes reactive groups that were previously engaged in internal bonding.

4.4. SDS-PAGE

SDS-PAGE profiles of the different protein isolates are shown in Fig. 3. The molecular weight of the keratin hydrolysate obtained (Lane 3) is similar to that of raw duck feathers (Lane 2), consistent with Woodin's findings [57], which suggest feather keratin is predominantly β-keratin. Prior studies estimate the molecular weight of chicken feather keratin to be around 10 kDa [58]. The results suggest preserving the

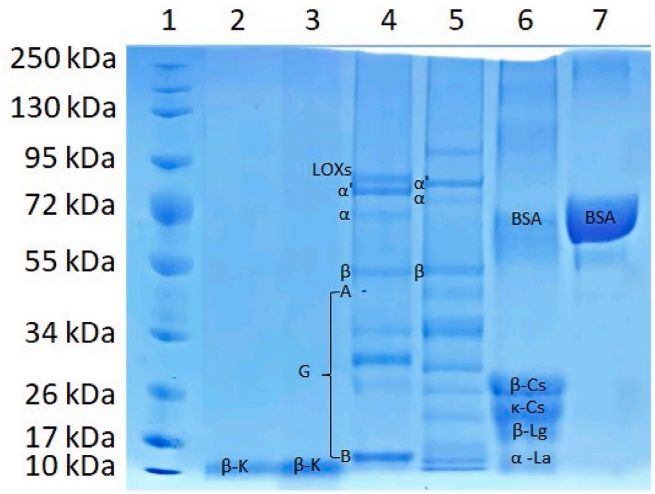

Fig. 3. SDS-PAGE of feather and protein isolates: Lane (1) prestained protein Ladder (10–250 kDa), Lane (2) raw feather, Lane (3) keratin hydrolysate, Lane (4) soybean, Lane (5) pea, Lane (6) casein, Lane (7) albumin standard.

original keratin structure during alkaline hydrolysis, which also agrees with other studies [59]. On the other hand, plant proteins in Lanes 4 and 5 have globulins and albumins as major components. 11S globulins and 7S globulins are the main components of glycinin and β-conglycinin in soy and pea proteins. 11S globulins (G, ≈320–400 kDa) is a hexamer consisting of different polypeptides in these plant protein isolates, and each subunit (≈60 kDa) comprises a basic subunit (B, ≈20 kDa) and an acidic (A, ≈40 kDa) bonded by a disulfide bond [26]. 7S globulins (≈150–200 kDa) are trimeric glycoproteins comprising several subunits associated with hydrogen bonding and hydrophobic rather than disulfide bonding. Soybean sample (lane 3) showed the band of α' (≈79 kDa), α (≈72 kDa), β (≈49 kDa) subunits of 7S β-conglycinin fraction, basic (≈13 kDa) and acidic (≈35 kDa), α + β (≈31 kDa), α + β + γ (≈49 kDa) of 7S vicilin, convicilin (≈72 kDa), and lipoxygenase (LOXs, ≈88 kDa). Pea sample (lane 4) showed α' (≈82 kDa), α (≈75 kDa), β (≈49 kDa), subunits of 7S β-conglycinin fraction, basic (≈12 and ≈ 15 kDa) and acidic (≈35 and ≈ 41 kDa), α + β (≈30 kDa), α + β + γ (≈49 kDa) of 7S vicilin, convicilin (≈75 kDa), and lipoxygenase (LOXs, ≈101 kDa) [60–62]. In general, 7S globulins exhibit a higher carbohydrate content when compared to their 11S counterparts [63], whereas 11S globulins are notably more abundant in protein content than 7S globulins [64]. Consequently, this distinction suggests that 7S globulins may have a greater tendency to participate in hydrogen bond interactions, while 11S globulins are disulfide-rich. As observed by SDS-PAGE, soybean proteins are more intense in 7S and have fewer bands in 11S than pea proteins. Casein (Cs) in Lane 6 exhibits bands from ≈10 kDa to over ≈200 kDa. These bands correspond to bovine serum albumin (BSA) Lane 7 (≈66 kDa), β -Cs (≈26 kDa), and κ-Cs (≈19 kDa), in addition to β-lactoglobulin (β-Lg, ≈18 kDa) and α-lactalbumin (α –La, ≈13 kDa), which are the main protein fractions found in whey protein [65]. This indicates that the hydrolysate is not pure protein. In literature, the chemical complexes between milk proteins (whey and casein) are known as co-aggregates of milk proteins; these can be present according to the interaction of both during isolation (time and temperature) [66]. Namely, after the use of 2-mercaptoethanol, the least intensive bands (≈190 kDa and ≈112 kDa-bands) suggest that these co-aggregates may have degraded and disappeared almost completely [67], resulting in the increase of the contents of β-Lg and α–La soluble forms along with κ-casein which show more intensive bands. BSA, β-Lg, and α –La all have disulfide bridges, and are known as effective sites to bind calcium or sodium when present [68].

4.5. MALDI-ToF-MS

The different proteins were analyzed by Matrix-assisted laser desorption ionization-time of flight (MALDI-ToF) mass spectrometry, and the results are presented in Fig. 4. Spectra of different mass ranges were acquired. A low range (0.5–5 kDa) is in reflector mode, and a high range (1–50 kDa) is in linear mode. It can be observed the distinct profiles of the different proteins, in which keratin, as previously shown in SDS-PAGE, had only a narrow molecular weight distribution with no high *m/z* peaks, correlating to lower viscosity in alkaline dispersions, possibly due to the smaller peptide sizes that may lead to less entanglement and intermolecular interaction. However, these low molecular weight peptides can penetrate the wood structure more efficiently, and this characteristic is a positive difference compared with the other food proteins. In contrast, casein, soybean, and pea proteins show clearly higher molecular weight peaks, aligning with their higher viscosity in dispersions, which could be attributed to larger protein fragments contributing to a denser network structure.

4.6. Effect of pH and viscosity

Viscosity plays a pivotal role in both adhesive application and bonding strength. The optimal viscosity enables easy and even application, avoiding problems like poor spreadability with high viscosity or weak bonding caused by excessive penetration with low viscosity. Moreover, viscosity variations, crucial for understanding adhesive behavior before hardening, are influenced by the protein's chemical and physical structure, including intermolecular forces and polymer chain behavior. Proteins at pH 8 and 9 tend to maintain their secondary structure, with protein chains mostly folded, keeping functional groups inaccessible [69]. Adjusting alkali concentrations revealed that lower hydroxyl concentrations resulted in a viscous and agglomerated consistency, while higher concentrations (pH 10 and 11) led to better uniformity with a more gel-like structure as proteins began to unfold and interact more freely. Optimal rheological behavior for adhesive flow was

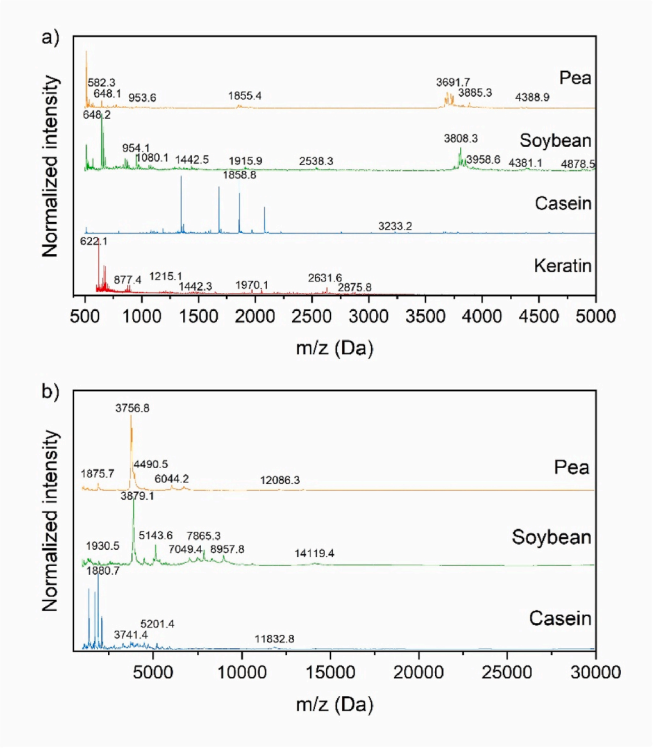

Fig. 4. MALDI-ToF Mass Spectrometry profiles of keratin, casein, soybean, and pea proteins at low and high mass ranges.

achieved at pH 12 (Table 1 and Fig. 5), where proteins fully unfold, exposing functional groups for interaction through van der Waals forces, hydrogen bonds, and disulfide bridges. However, at pH 13, lower viscosities were obtained, indicating excessive hydrolysis and shortening of the protein backbone. This implies that pH levels should ideally be maintained below 13 to avoid poor bonding and high water absorption [69].

Moreover, the study reveals that viscosity varies with protein content and alkali type in two different phenomena; excess alkali can either increase viscosity by unfolding proteins and increasing the friction among them or decrease it by breaking proteins into smaller chains, resulting in overpenetration into wood. The viscosity of the adhesive is also dependent on solid content, where a balance between adhesive flow, ability to wet, penetration, and water evaporation is necessary, especially for cold-set adhesives. In the case of protein-based adhesives, the operating viscosity limits range from 0.5 to 75 Pa s, depending upon the nature of the materials to be bonded. A viscosity of 0.5–5 Pa s is needed for bonding materials that are highly absorbing, such as paper, soft board, and dried wood aggregates, 5–250 Pa s for most wood laminating purposes (both cold or hot press), and over 500 Pa s for mastic consistency wood laminating operations [69]. In the 40 formulations established (Fig. 5), the lower protein content generally showed lower viscosities, with sodium (Na) alkalis lower viscosities than with calcium (Ca) alkalis are obtained due to NaOH's stronger alkali nature and its higher pH levels. Calcium's chelation with protein carboxyl groups also forms insoluble compounds, increasing viscosity [38]. This particularly was shown in the case of K-1.5-Ca-0.2 being less viscous than K-1.5-Ca-0.5, C-1.5-Ca-0.2 less viscous than C-1.5-Ca-0.5, and P-1.5-Ca-0.2 less viscous than P-1.5-Ca-0.5. These formulations also had similar pH levels, meaning that calcium does not affect the pH, being a weaker base ($pK_B = 1{,}37$) than NaOH ($pK_B = -2{,}43$) and less soluble.

In contrast, Na-based formulations generally exhibited lower viscosities at higher concentrations, except in cases like S-2-Na-0.2 being less viscous than S-2-Na-0.5, likely due to the excess alkali unfolding and increasing friction among protein molecules. Regarding proteins, keratin displayed the lowest viscosity, allowing for higher solid content in formulations. This probably arises from two different causes. Firstly, the higher viscosity in the more polar proteins (casein, soybean, and pea) is governed by intermolecular forces that enable them to form hydrogen bonds with the alkali solvent. Secondly, the strength of these interactions between proteins and the alkali solvent directly correlates with the solubility of the proteins. In this context, keratin was observed to be less soluble, forming aggregates more readily compared to the other proteins [70]. The diverse colors of protein-based adhesives treated with NaOH and $Ca(OH)_2$, as observed in Fig. S2, likely confirm the distinct chemical interactions these alkalis have with protein structures. NaOH may preferentially disrupt disulfide bridges, exposing thiol (-SH), which oxidizes and may contribute to color changes. Conversely, calcium hydroxide forms stable complexes with carboxyl groups, leading to larger particles that scatter light differently, resulting in a matte appearance compared to the more transparent adhesives obtained with NaOH.

4.7. Dielectric analysis

The cure behavior of the different protein-based adhesives was assessed using dielectric analysis (DEA), as illustrated in Fig. 6, a technique that provides valuable insights into changes in ion viscosity, which directly correlates with the adhesive's transition from an uncured to a cured state at room temperature.

Ion viscosity is a critical indicator of the adhesive's curing progress, reflecting the mobility of ions within the adhesive. The adhesive's composition significantly influences this mobility. Within the initial minutes, the adhesive's structure is less organized, which leads to a lower ion viscosity before the start of polymer chain crosslinking (Fig. 6a, phase A) [71]. Polymerization reactions and chain growth rapidly counteract this phenomenon, resulting in a significantly higher final ion viscosity and reduced ion mobility, indicating curing has begun (Fig. 6a, phase B).

The ion viscosity is usually represented on a logarithmic scale [71]. It is observed that curing times differ depending on the type of protein used and the alkali employed. In the case of $Ca(OH)_2$, the curing time varies slightly among proteins but generally falls within the range of 300–400 min. This is faster than in the case of NaOH. The slowest curing time was observed with keratin (900 min), followed by casein (600 min), while soy and pea exhibited similar behavior (500 min). This trend agrees with the trend observed before in the viscosity test. This linear increase culminates at a maximum point due to vitrification. This indicates the transition of the adhesive from a liquid state to a solid state, where the molecules within the adhesive become immobilized and cured (Fig. 6a, phase C). Notably, the maximum viscosity achieved depends more on the type of alkali used. In the case of NaOH, the maximum viscosity achieved was lower for all proteins than for Ca $(OH)_2$, as formulations with NaOH exhibited lower viscosity (Fig. 5).

4.8. Water interaction after curing

The study of the water contact angle on protein adhesives underscores the role of polar or charged amino acids in increasing protein interaction with polar surroundings. This is achieved by burying hydrophobic amino acids into the core (hydrophobic effect) and establishing hydrogen bonds via hydrophilic residues with water or polar surface to minimize free energy [72,73]. The solubility and stability of proteins are affected by many extrinsic factors, such as pH, solvent, and metal ions [74]. The interaction between proteins and wood surfaces involves similar hydrogen bonding mediated by the protein's polar amino acids and wood's polar groups (hydroxyl groups), particularly in an aqueous environment comprising water and charged cations [75]. According to Fig. 7, the treatment with NaOH enhances the hydrophilicity of protein adhesives compared to $Ca(OH)_2$, likely due to NaOH's stronger base properties leading to stronger denaturation and exposure of hydrophilic groups. Notably, casein showed the highest

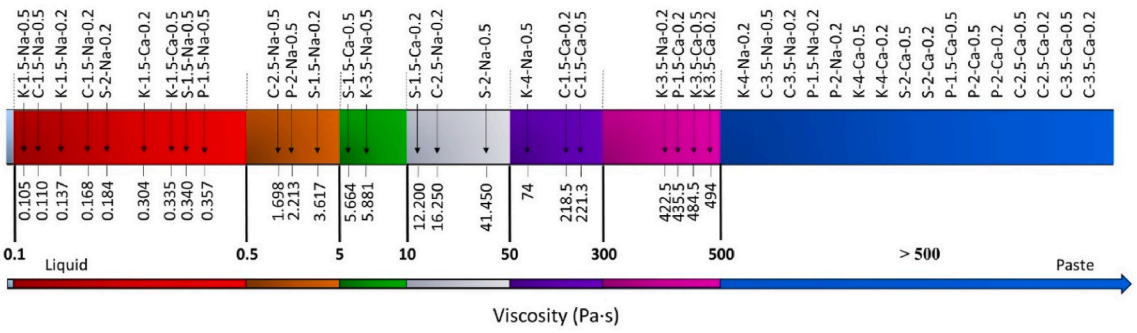

Fig. 5. Viscosity of the 40 protein-based formulations.

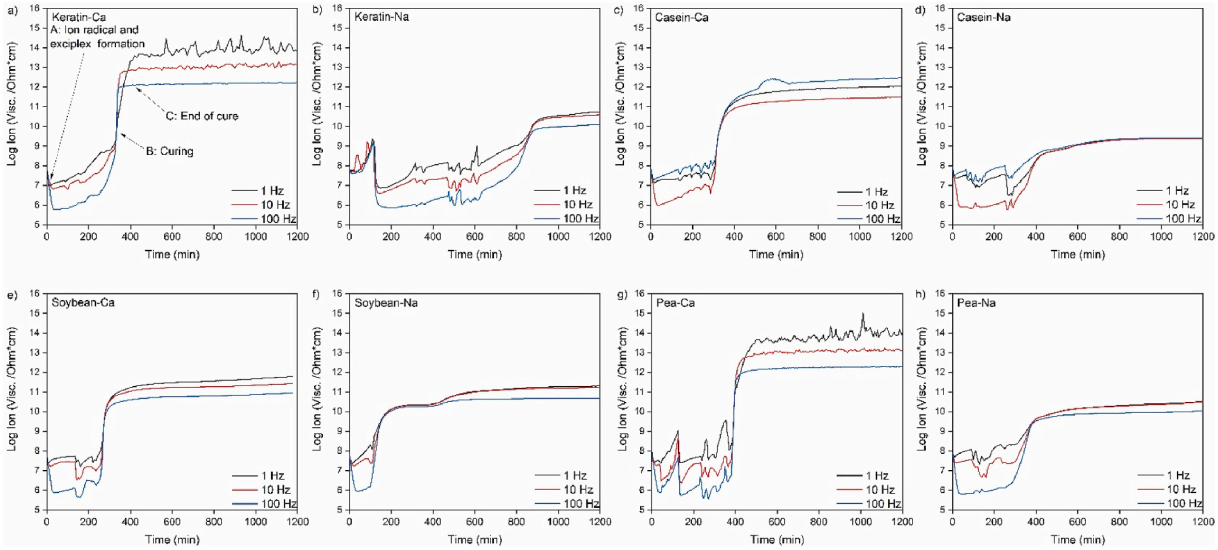

Fig. 6. Dielectric analysis of different protein-based formulations.

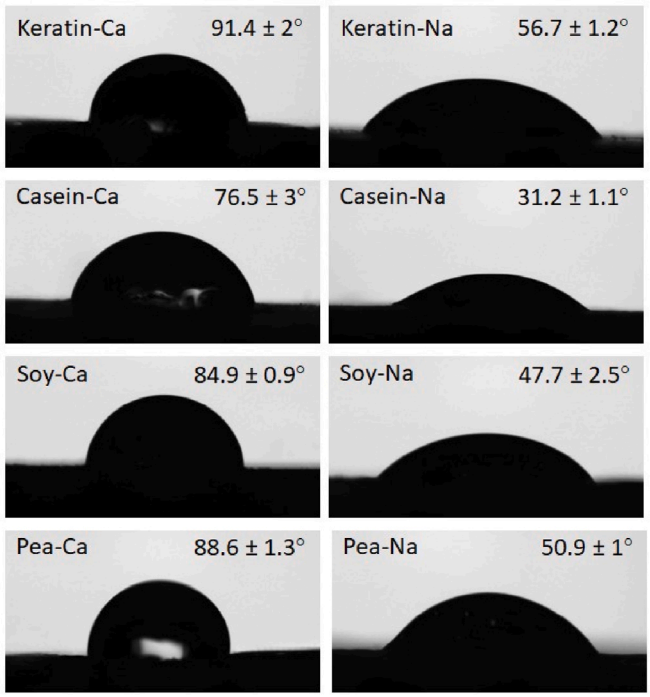

Fig. 7. Contact angle of water droplets on the surface of different protein adhesives after drying.

hydrophilicity, which agrees with previous studies at pH range from 6 to 12, due to increased negative charge and electrostatic repulsion at higher pH levels [76]. While calcium ions typically stabilize casein by bridging interactions, adding $Ca(OH)_2$ might reveal non-polar areas [77]. However, whey and albumin, which do not form similar structures, help maintain a hydrophilic surface [78]. The presence of κ-casein also increases and extends from the casein micelles, giving it a layer stabilizing the micelle in solution and preventing further aggregation [79].

Many intra- and intermolecular disulfide crosslinks and other structural features stabilize keratin. Its strength and stiffness are due to the high proportion of cysteine residues in the polypeptide backbone, bonded by disulfide links [80]. Moreover, cysteine is the monomer most frequently found in the core and thus represents the most markedly hydrophobic amino acid [81]. In soybean proteins, their hydrophilicity is linked to the exposure of hydrophilic groups upon unfolding, as indicated by their higher content of carbohydrate-rich 7S globulins in SDS-PAGE, which can be able to establish more hydrogen bonds compared to pea proteins. Less hydrophobicity on the surface of the protein may lead to higher polar interactions, which promote protein-water interactions or protein-wood interactions.

4.9. *Thermal and flammability analysis*

The low flammability and thermal stability of protein-based adhesives, including keratin, are gaining attention as indoor safety and environmental sustainability regulations increase. This push aligns with the global drive towards carbon neutrality and the demand for halogen-free, eco-friendly flame retardants [82]. This study explores the thermal behavior and decomposition of protein-based adhesives, focusing on their potential to form protective char.

DSC is essential in this analysis for measuring protein denaturation, which impacts secondary and tertiary structures, such as α-helix and β-sheet. This can be detected through changes in heat capacity as proteins unfold, often marked by an endothermic peak. The process mainly disrupts hydrogen bonds, hydrophobic and ionic interactions, and occasionally disulfide bridges. The DSC curves of feathers and different protein isolates are presented in Fig. 8a. The first endotherm peak at 100–150 °C indicates water desorption and protein unfolding due to hydrogen bond disruption, noted as critical morphological changes in Fig. 8a [83]. It should be noticed that, generally, crosslinking induces a reduction in melting enthalpy systems because of both a decrease in the hydrogen bonds forming the microstructural network, which breaks endothermically and a simultaneous increase in the extent of covalent crosslinks, which exothermic ruptures [84]. In the case of keratin, the hydrogen bonding between water molecules and the keratin structure requires the temperature to exceed 100 °C to evaporate. In contrast, the other proteins indicate a higher number of hydrogen bonds, which are the main interactions for maintaining casein micelles, in addition to the 7S globulins, which were more intense in soy protein hydrolysate than pea.

In the range 200–250 °C, feathers and keratin show a major endotherm due to α-helix decomposition and disordering (in other works, this transition is also described as a "melt"), revealing that the feather keratin liquefies at temperatures from 210 to 240 °C [85]. In this range, keratin shows distinctively broader denaturation, suggesting the gain of

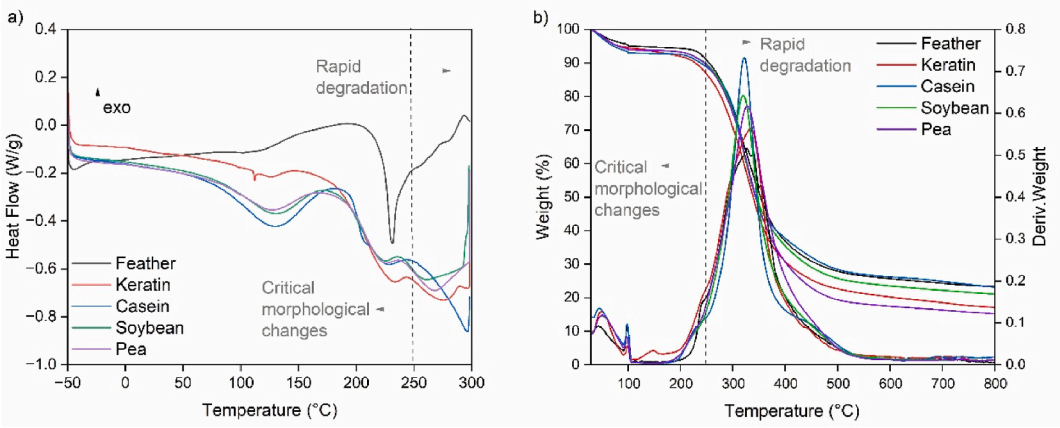

Fig. 8. Left: DSC of feathers and different protein isolates. Right: TG and DTG curves of the feathers and different protein isolates; the arrow indicates the primary structure destruction started.

amorphous behavior and loss of α-helix structures, as indicated by earlier IR spectrum analysis. Casein exhibits a two-phase denaturation in this range, likely reflecting the different thermal stabilities of β and κ caseins. Soybean and pea both showed a single-phase denaturation, which could correspond to the thermal denaturation of their respective 7S globulins, higher in soybean as indicated in earlier SDS-PAGE analysis. In the range 250–300 °C, noted as rapid degradation in Fig. 8a, feather and keratin undergo two-phase decomposition, with keratin displaying higher stability up to 298 °C due to β-sheet followed by the degradation of disulfide bonds. Similarly, casein shows an endothermic peak at 295 °C, indicating disulfide degradation in BSA, β-Lg, and α –La. In soybean and pea proteins, the peaks at 255 °C and 265 °C could indicate the breakdown of the more complex structures as the 11S globulins, which are more pronounced in pea proteins.

Thermogravimetric analysis can detect protein degradation, which involves breaking chemical bonds within the material and changing its chemical structure. The degradation region was separated into two regions in the analysis: a low-temperature region ($T < 250$ °C) where critical morphological changes occur (highlighted with an arrow in the differential thermogravimetric (DTG) plots in Fig. 8b and a high-temperature region ($T > 250$ °C) where rapid degradation occurs. At $T < 250$ °C, the initial weight loss of all samples due to free water desorption was evident at 100 °C. The water desorption was followed by a plateau roughly up to 150 °C in the case of keratin, confirming the release of bound water as shown in DSC. Total water desorption for all proteins was around 5–7%. A noticeable change in slope of the DTG at ≈230 °C in feathers is due to α-helix disordering breakdown, similarly for keratin, which was less pronounced due to less α-helix as shown before. For casein, the slope change could be attributed to the degradation of κ and β casein, which may be due to their micellar structure of weaker interactions. The slope change starts at around 235 °C for pea and soybean proteins, corresponding to the degradation of 7S globulins stabilized by non-covalent bonds.

In the second range ($T > 250$ °C), feathers show the slowest degradation rate, followed by keratin, indicating β-sheet and cystine degradation, likely due to their more complex structures and char formation, which acts as a barrier to further degradation, as confirmed in previous studies [86]. Casein exhibited the fastest degradation, noted by the highest DTG peak, likely from disulfide bridge cleavage in BSA, β-Lg, and α-La, and a high hydrogen bond content. Soybean and pea proteins degraded more slowly, which is attributed to the thermal stability of 11S globulins, especially in pea proteins that contain more 11S globulins. The degradation rate generally followed the hydrogen bond content, with casein degrading fastest, then soybean, pea, keratin, and feathers in the 300–400 °C range. Regarding residue formation, feathers yield the highest (23.37%), suggesting substantial carbonaceous residue from their complex, cystine-rich structure. Casein follows with significant residue (23.12%), likely from its mineral and salt content. Soybean (21.10 %) and keratin residues (17.11%) are lower, with keratin's purity influencing its residue levels. Pea protein leaves the least residue (15.17%), possibly because its ester groups promote the release of volatiles upon heating.

Fig. 9 presents the micro combustion calorimetry (MCC). It is important to retain four major aspects from this analysis; the first is the Peak Heat Release Rate (Peak HRR, W/g), which measures the maximum rate at which a sample releases heat per unit mass during combustion. Second is the temperature of peak heat release rate (TPHRR, °C), the temperature of peak HRR occurrence. Then is the Total Heat Release Rate (Total HRR, kJ/g), representing the total energy released per unit mass of the sample during combustion in the analyzed temperature range. Last is the Char Yield (%): This refers to the percentage of residue remaining after a material has been completely combusted or pyrolyzed. Peak heat release rate (HRR) is one of the most important parameters used to evaluate the flammability of materials.

The micro combustion calorimetry provided critical insights into the thermal decomposition and flammability of the different protein isolates, both untreated and alkaline-treated, as seen in Fig. 9a and the corresponding data in Table S2. The MCC results of feathers and keratin showed a two-peak heat release rate (HRR). Based upon this two-peak HRR curve and the visual observation of char formation, it can be said that these specimens behave like charring materials. Once the upper char layers are thermally damaged, volatiles and gases like hydrogen sulfide start to be released, and following further disulfide bond interactions, char formation ensues, and the underlying material burns away, leading to a second peak of HRR. The formation of a strong char layer can prevent the substrate from decomposing into small molecules [86]. The final chars for the samples were black, hard, and difficult to burn or clean (Figure S4). The other difference from other proteins can also be the significant presence of cystine, which is generally considered to contribute to the folding and stability and, therefore, the relatively lower flammability of the feathers compared to Keratin. However, the crosslinked structure of keratin, due to disulfide bonds still, makes its thermal degradation more complex and potentially less volatile and calorific compared to casein, which shows the highest PHRR (222 W/g) with a narrow peak due to the release of gases like carbon dioxide, ammonia, and possibly other sulfur-containing gases. The specific structure of casein might lead to a rapid release of these gases within a narrow temperature range, leaving a more developed and porous char structure (Fig. S4).

Soybean and pea proteins showed similar behavior, with more complex combustion, which can be due to 7S and 11S globulins. Moreover, a blackened char with no morphological changes, which was

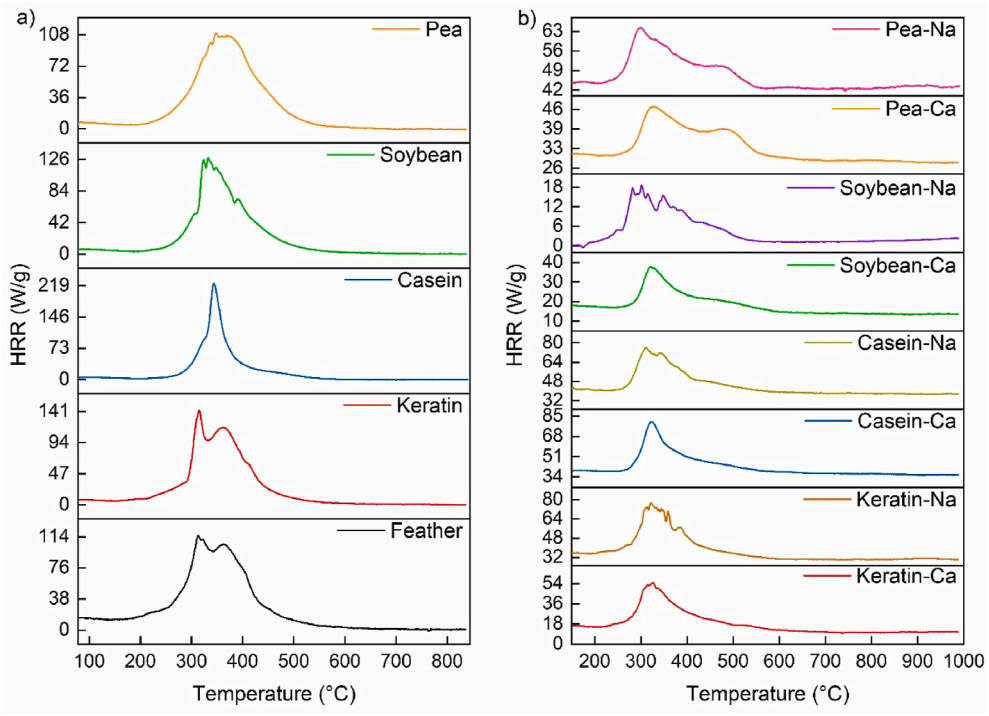

Fig. 9. Microcombustion calorimetry data for the different samples under aerobic conditions.

quite fragile and easily broken, was obtained (Fig. S4). Interestingly, pea proteins show the highest flame retardancy due to the ester linkage in pea proteins, which can bring rigidity to their structures [87]. Overall, the flammability profiles of these proteins are characterized by relatively low peak HRR values when compared with those of epoxies and vinyl esters [88].

Upon alkaline treatment (Fig. 9b) and the corresponding data in Table S3, it is interesting that all NaOH proteins exhibited lower degradation temperatures than $Ca(OH)_2$. Regarding chemical structure and stability, the interaction of $Ca(OH)_2$ may lead to complex formations, as Ca^{2+} ions bind with carboxyl groups in the protein's structure. This results in a more stable compound that undergoes uniform decomposition, as evidenced by the smoother HRR curve and higher char yields than NaOH formulations (Table S3). In contrast, NaOH might be causing the formation of less stable intermediates that decompose at different rates, resulting in multiple peaks in the HRR profile. The Keratin-Ca formulation exhibited the highest char yield compared to other proteins, confirming its ability to form a more stable char during combustion.

On the other hand, NaOH is presumed to disrupt these disulfide bonds, reducing more cystine to cysteine and potentially leading to a complex series of degradation steps, as reflected in the multiple HRR peaks. A notable two-peak HRR behavior was observed in some proteins, like pea protein, but was absent in soy proteins after alkaline treatment. Intriguingly, pea proteins displayed this distinctive pattern, not replicated in their soy counterparts. This divergence points towards the unique chemical composition of pea proteins, which contain esters that potentially foster stable crosslinking interactions under alkaline conditions, leading to enhanced thermal stability and the subsequent second peak in the HRR graph at around 500 °C. The absence of such ester linkages in soy proteins could explain their lack of a similar second peak in thermal analysis.

5. Mechanical tests

In assessing the lap shear strengths of adhesives derived from casein, soybean, pea, and keratin proteins when dispersed in NaOH and Ca $(OH)_2$ (Fig. 10), it is observed that the proteins ranked in terms of strength from highest to lowest as casein, soybean, pea, and keratin, for both NaOH and $Ca(OH)_2$. This ranking aligns with the proteins' hydrogen bond content, indicating hydrogen bonding as a primary adhesion mechanism, with proteins forming crosslinks with wood's hydroxyl groups. In addition, all proteins exhibited improved adhesion with increased protein content, except for casein at a 3.5% solid content, likely due to optimal functional group exposure and viscosity. Wood fiber tear-out was obtained in all samples exceeding 8 MPa (Fig. S5 and Fig. S6).

The ANOVA analysis of the mechanical properties of the adhesive formulations is displayed in Table S4, indicating the influence of several factors on their significance and performance by classifying them according to shared characteristics that affect their performance. Among the factors is the viscosity, with formulations sharing similar viscosity profiles—grouped as (l, m, and n) (Table S4)—demonstrating comparable wood penetration and wetting capabilities, hence similar mechanical strengths. This group includes K-3.5 and K-4 similar to the viscosities of C-1.5-Na-0.2, all pea formulations except P-1.5-Ca-0.5 and P-2-Na-0.2, all soybean formulations except S-1.5-Na-0.5, and S-2 formulations. Another factor can be hydrogen bonds, where formulations that can form a similar number of hydrogen bonds with the wood's hydroxyl groups would be expected to show no significant difference in mechanical strength. This insight led to the classification of groups (e, f, g, h, i, j, and k) (Table S4), encompassing all formulations of 1.5 g protein and 0.5 g $Ca(OH)_2$ excepting keratin formulations, which showed far hydrophilicity values in the contact angle. Moreover, the 'o' groups (o and p) (Table S4) of K-1.5, K-3.5, and P-1.5-Ca-0.5 can be due to low viscosities and insufficient hydrogen bonds.

In more detail, casein shows the highest adhesive strength, significantly enhanced by NaOH's ability to reveal functional groups, facilitating hydrogen bonding. However, its strength decreased with higher $Ca(OH)_2$ concentrations, possibly due to calcium complexation causing steric hindrance and increased viscosity, which could hinder protein-wood interlocking. Soybean protein was second in strength and preferred NaOH, likely due to its solubility and reactive site exposure. Higher NaOH concentrations corresponded with stronger lap shear

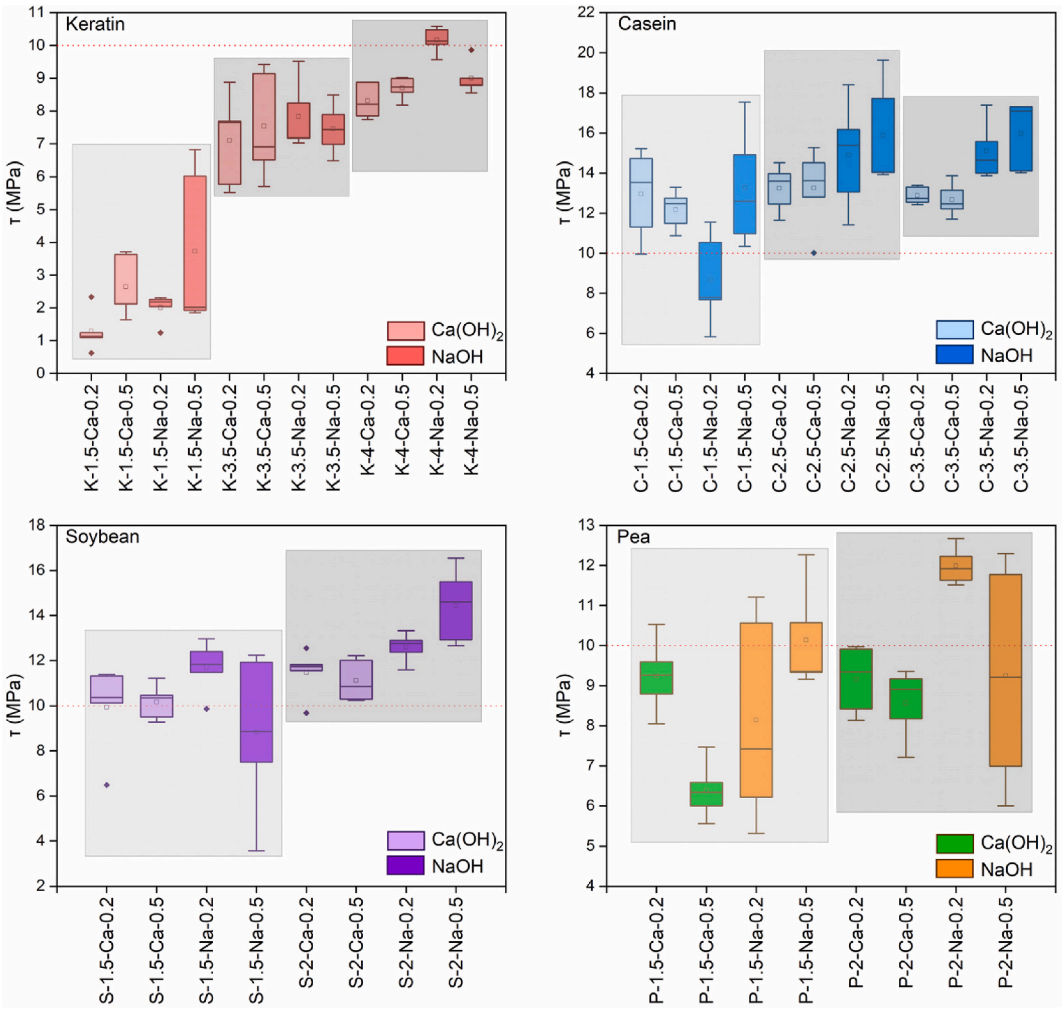

Fig. 10. Mechanical properties of alkaline-treated protein adhesives: Lap-shear test results on wood according to EN205; red dotted line indicates minimum requirement for indoor applications.

strengths, suggesting optimized protein-wood interaction. Conversely, increased $Ca(OH)_2$ viscosity might disrupt adhesive layer uniformity, weakening the bond. Pea protein adhesives performed better with lower alkaline concentrations. This indicates that pea proteins are possibly more susceptible to alkali-induced degradation, compromising adhesive strength. While $Ca(OH)_2$ could induce crosslinking, the resultant steric hindrance and rise in viscosity appeared to counteract any strength benefits.

Keratin met minimum requirements with lower NaOH concentrations and maximum protein content, suggesting a balance between reactive site exposure and protein integrity. Interestingly, increased $Ca(OH)_2$ concentrations did not reduce strength, indicating less impact of calcium complexation on keratin's adhesive properties. The presence of elemental sulfur might affect keratin's reactivity and crosslinking capability. The larger disruption of disulfide bonds in NaOH could lead to a more extended keratin chain, which may increase its interaction with wood hydroxyl groups. Additionally, highly nucleophilic and reactive thiolates are capable of forming covalent bonds with electrophilic centers like the aldehyde groups present in the lignin component of wood [89]. Lap shear strength results indicate that NaOH is generally more effective than $Ca(OH)_2$ in formulating protein-based wood adhesives due to better protein solubility, dispersion, and wood surface modification, which facilitate more effective hydrogen and ionic bonding without the adverse effects of complexation and steric hindrance observed with $Ca(OH)_2$.

6. Physical tests

The physical properties of the different protein-based adhesives were assessed, focusing on the potential reactions between alkalis and protein molecules using ATR-IR (Fig. 11a). The spectra reveal distinct alterations in main functional groups due to alkali treatment compared to pure proteins (Fig. 1) (see Fig. 12).

The increased bands around 1085-1035 cm^{-1} are attributed to the bending vibrations of hydroxyl (OH) groups from $Ca(OH)_2$ and NaOH, indicating interactions with the protein structures. The increase at 1388 cm^{-1} C–H bending vibration suggests changes in methylene groups' environments due to protein unfolding. The broadening of the Amide II band indicates increased hydrogen bonding and protein unfolding, disrupting the secondary structure and creating a varied environment for N–H bending and C–N stretching. Changes in the symmetric and asymmetric stretching of C–H bonds in methylene groups at 2877 and 2922 cm^{-1} suggest further structural alterations and transformation to amino acids with alkyl side chains. Concurrent bands of both NaOH and C a$(OH)_2$ in the 2954-2850 cm^{-1} region support these alterations. The broadening of the absorption band around 3295 cm^{-1} indicates increased O–H and hydrogen bonding, suggesting reactions with OH and NH groups, enhancing adhesive properties. The bands between 3640 cm^{-1} and 3685 cm^{-1}, characteristic of hydroxyl groups from $Ca(OH)_2$ and NaOH, indicate the incorporation of these alkali hydroxides into the protein structures.

Although all protein-based adhesives maintain their main structure

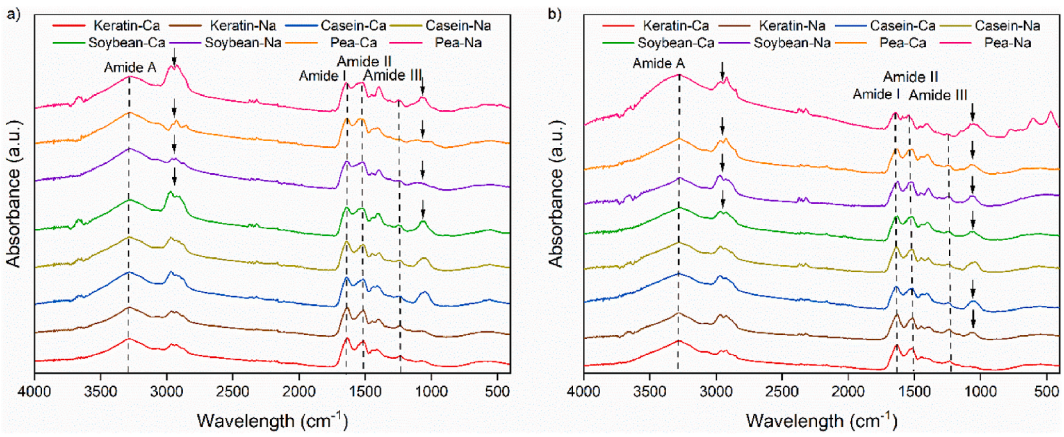

Fig. 11. ATR-IR spectra of protein-based adhesives before (a) and after (b) the sol-gel test. Amide A, I, II, and III regions are marked by dashed lines, with arrows indicating changes for comparison.

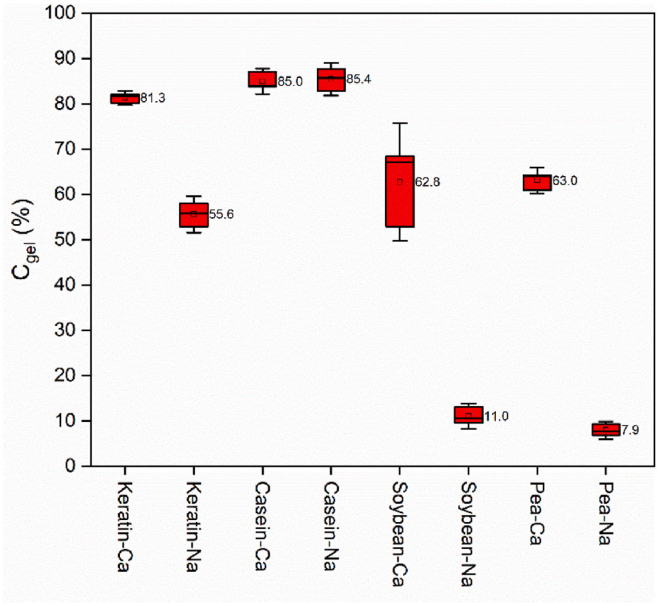

Fig. 12. Gel content percentage of the different protein-based adhesive samples.

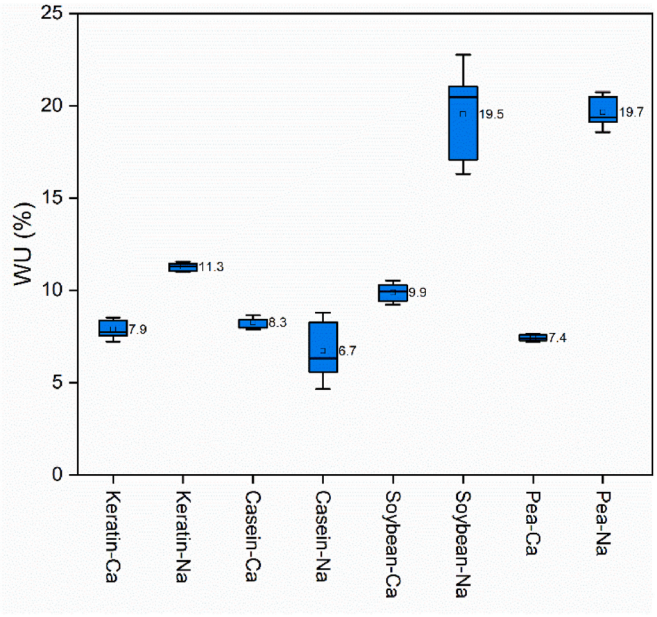

Fig. 13. Water uptake percentage of the different protein-based adhesive samples.

(Amide A, I, II, and III bands) after alkali treatment, the analysis of the Amide I band using curve fitting (Table S5 and Fig. S7) revealed significant changes in protein secondary structures after alkaline treatment with NaOH or $Ca(OH)_2$. The percentage of aggregate strands decreased across all proteins. For instance, Keratin-Ca decreased to 12.79% and Keratin-Na to 10.75%, compared to pure Keratin at 16.79%, while Pea-Ca retained a higher percentage (12.95%) compared to Pea-Na (5.81%). The β-sheet (inter. AP) content significantly decreased for all proteins, with Casein-Ca and Casein-Na dropping to around 23% from pure casein's 28.34%. Soybean adhesives exhibited a notable reduction in β-sheet (inter. AP) content, with NaOH treatment reducing it to 22.13% from 32.42% in its pure form. This reduction suggests alkaline treatments break down intermolecular β-sheets, leading to a more dispersed protein structure.

On the other hand, the intramolecular β-sheets (β-sheet (intra. P)) percentage increased across all proteins, indicating a restructuring into more intramolecular interactions. For instance, Keratin-Ca and Keratin-Na increased to 27.97%, compared to pure Keratin at 22.45%. The α-helix content increased for all proteins except Keratin. Casein-Ca and Casein-Na rose to 18.17% from pure casein's 14.15%, with Pea-Ca showing a significant increase to 20.36%. This increase indicates that alkaline treatment allows some protein regions to refold into α-helical structures, although keratin's high cysteine content might inhibit this refolding. Furthermore, there was an increase in β-turn/random coil content across all proteins, reflecting greater flexibility and less ordered nature post-treatment. For example, Pea-Ca increased to 13.38% and Pea-Na to 16.29%, compared to pure pea at 9.39%. Similarly, keratin and soybean proteins showed increased random coil content after treatment. The β-sheet (inter AP)/side chains content showed slight changes, generally decreasing or changing minimally, with Pea-Ca retaining the highest percentage (5.92%) post-treatment. This minimal change suggests that side-chain interactions are less affected by alkaline treatment. Alkaline treatments reduce aggregate strands and intermolecular β-sheets while increasing intramolecular β-sheets, α-helices, and random coils. NaOH treatment results in more significant denaturation and less structured proteins than $Ca(OH)_2$, which better preserves secondary structures.

7. Sol-gel test

The gel content (C_{gel}) reflects the crosslinking density of the adhesives. Higher values indicate more extensive crosslinking and better stability. Sol-gel tests assessed the curing behavior of protein-based adhesives treated with NaOH and $Ca(OH)_2$, with ATR-IR spectra revealing structural changes.

Keratin treated with $Ca(OH)_2$ showed higher gel content (81.3%) compared to NaOH (55.6%), suggesting more effective crosslinking due to stabilization of the keratin structure by calcium ions forming strong ionic bonds. Keratin's high cysteine content, which forms disulfide bonds, contributes to its strong network structure, although it is less effective with NaOH. Both alkali treatments resulted in high gel content for casein-based adhesives, indicating extensive crosslinking (85.0% for Casein-Ca and 85.4% for Casein-Na). Casein, the most hydrophilic with multiple polar and reactive groups, forms extensive hydrogen bonds and interacts effectively with NaOH and $Ca(OH)_2$, leading to a tightly packed, water-resistant network. Soybean adhesives, with moderate hydrophilicity, have fewer reactive sites for hydrogen bonding compared to casein but more than keratin. This intermediate level of hydrophilicity and functional groups like amines and carboxyls allow for a reasonable degree of crosslinking. The C_{gel} values of 62.8% (Soybean-Ca) and 11.0% (Soybean-Na) suggest that $Ca(OH)_2$ induces better crosslinking than NaOH, possibly due to the formation of stronger ionic bonds and less protein denaturation. Pea protein has the lowest hydrophilicity among the non-keratin proteins, resulting in fewer sites for hydrogen bonding. This lower reactivity limits the extent of crosslinking that can occur. The C_{gel} values of 63.0% (Pea-Ca) and 7.9% (Pea-Na) reflect this limitation, showing that while $Ca(OH)_2$ can still induce crosslinking, the overall network is not as strong as that of casein or keratin.

ATR-IR spectra after the sol-gel test (Fig. 11b) showed that keratin and casein-based adhesives remained similar before and after the test, with slight increases in bands at 1055 cm^{-1} due to exposed hydroxyl groups. Soybean and pea adhesives exhibited significant spectral changes, with increased bands at 1055 cm^{-1} in Soybean-Na, Pea-Ca, and Pea-Na, and decreased in Soybean-Ca. The decreased bands in the 2954-2850 cm^{-1} region suggest that salts were washed out after the sol-gel test, especially with NaOH treatment, reducing crosslinking sites and stability.

8. Water uptake test

The water resistance of different protein-based adhesives is crucial for maintaining the stability and mechanical properties of artificial boards under humid and warm conditions. The adhesives were tested at 50 °C and 80% relative humidity, and the water uptake (WU) value was measured. Lower WU indicates better water resistance, which aligns with the degree of crosslinking observed in the sol-gel tests. Due to weak intermolecular forces, adhesives with low crosslinking decompose and dissolve easily in water. In contrast, highly crosslinked adhesives form strong network structures that resist water invasion, reduce solubility, and enhance water resistance.

Keratin treated with $Ca(OH)_2$ showed lower water uptake (7.9%) compared to NaOH treatment (11.3%), indicating better water resistance and higher crosslinking. Casein-based adhesives had low water uptake for both treatments (8.3% for Casein-Ca and 6.7% for Casein-Na), reflecting good water resistance and extensive crosslinking. Soybean adhesives treated with $Ca(OH)_2$ had significantly lower water uptake (9.9%) compared to NaOH treatment (19.5%), indicating superior crosslinking and stability with $Ca(OH)_2$. Pea-based adhesives showed similar trends, with $Ca(OH)_2$ treatment resulting in lower water uptake (7.4%) compared to NaOH (19.7%), indicating better water resistance and crosslinking.

Overall, the water resistance properties of the protein-based adhesives, as indicated by WU, align well with the sol-gel test results. Ca $(OH)_2$ treatment generally provides better crosslinking and water resistance than NaOH treatment.

9. Conclusions

This work studied the development of sustainable wood adhesives from waste proteins like keratin from duck feathers, providing an eco-friendly alternative to traditional petroleum-based adhesives and aligning with the increasing demand for sustainable industrial practices. Utilizing keratin, a byproduct usually undervalued showcases an approach to wood bonding technology from the circular economy and green chemistry perspectives. The results indicate that hydrogen bonding is the key mechanism for adhesion between these proteins and wood. Using NaOH to treat proteins increased their solubility and exposed functional groups more effectively than $Ca(OH)_2$, thus indicating its superior efficiency in preparing proteins for adhesive use, resulting in stronger wood bonding. Post-alkaline treatment not only improved the solubility but also influenced the secondary structure of the proteins, enhancing their ability to form crosslinks. This enhancement was particularly evident in the improved gel content observed in the sol-gel tests, highlighting the increased degree of crosslinking, contributing to the adhesive strength and durability. Keratin-based adhesives stand out because they support higher solid content with less water, reducing the energy needed for curing. The high cysteine content in keratin, forming disulfide bridges, imparts thermal stability and potential fire resistance. The formation of a char layer under fire conditions can retard fire spread, enhancing the safety of keratin-adhered materials, as shown in MCC analysis. Additionally, the water uptake tests demonstrated that post-alkaline treatment resulted in a high crosslinking of the keratin-based adhesive with superior resistance to moisture compared to the other proteins. These advancements position keratin adhesives as a robust, environmentally sustainable alternative. This study mitigates environmental waste and presents a potential green substitute for conventional protein-based green adhesives using food-use proteins.

CRediT authorship contribution statement

Nidal Del Valle Raydan: Writing – original draft, Methodology, Investigation, Formal analysis, Data curation. **Katharina Richter:** Writing – original draft, Formal analysis, Data curation. **Bertrand Charrier:** Writing – review & editing, Supervision. **Andreas Hartwig:** Writing – review & editing, Validation, Supervision. **Eduardo Robles:** Writing – review & editing, Writing – original draft, Data curation, Conceptualization.

Declaration of competing interest

The authors declare the following financial interests/personal relationships which may be considered as potential competing interests: Eduardo Robles reports financial support was provided by French National Research Agency. Nidal Raydan reports financial support was provided by Nouvelle-Aquitaine Regional Council. If there are other authors, they declare that they have no known competing financial interests or personal relationships that could have appeared to influence the work reported in this paper.

Data availability

Data will be made available on request.

Acknowledgments

E.R. was supported by the Agence Nationale de la Recherche (ANR-16-IDEX-0002); N.R. got funding from the Conseil Régional Aquitaine (AAPR2020-8631210). Research mobility of N.R. to Bremen was funded

by the Doctoral School E211 and the Office franco-allemand pour la Jeunesse (Ref. 3631). The authors want to acknowledge the human and technical support provided by Fraunhofer IFAM technical staff (M.R., G. A., I.G., K.F., and C.W.).

Appendix A. Supplementary data

Supplementary data to this article can be found online at https://doi.org/10.1016/j.mtsust.2024.100905.

References

[1] H. Younesi-Kordkheili, A. Pizzi, A comparison among lignin modification methods on the properties of lignin–phenol–formaldehyde resin as wood adhesive, Polymers 13 (2021), https://doi.org/10.3390/polym13203502.
[2] B. Li, Z. Yuan, J. Schmidt, C.C. Xu, New foaming formulations for production of bio-phenol formaldehyde foams using raw kraft lignin, Eur. Polym. J. 111 (2019) 1–10, https://doi.org/10.1016/j.eurpolymj.2018.12.011.
[3] P. Antov, V. Savov, N. Trichkov, Ľ. Krišťák, R. Réh, A.N. Papadopoulos, H. R. Taghiyari, A. Pizzi, D. Kunecová, M. Pachikova, Properties of high-density fiberboard bonded with urea–formaldehyde resin and ammonium lignosulfonate as a bio-based additive, Polymers 13 (2021), https://doi.org/10.3390/polym13162775.
[4] S. Oktay, N. Kızılcan, B. Bengu, Oxidized cornstarch – urea wood adhesive for interior particleboard production, Int. J. Adhesion Adhes. 110 (2021), https://doi.org/10.1016/j.ijadhadh.2021.102947.
[5] J. Liu, H. Mo, E. Xie, J. Fang, Z. Hou, W. Gan, Utilization of carbon black from Mao bamboo as reinforcing agent for melamine urea formaldehyde resin wood adhesive, Ind. Crops Prod. 187 (2022), https://doi.org/10.1016/j.indcrop.2022.115373.
[6] EPA, LOCATING AND ESTIMATING AIR EMISSIONS FROM SOURCES OF FORMALDEHYDE (REVISED), 1991.
[7] J. London, G.F. White, A.C. Upton, Formaldehyde and cancer risk, Natl. Cancer Inst. (2011) 1–6.
[8] World Trade Organization, Committee on Technical Barriers to Trade, 2022.
[9] V. Duscha, J. Wachsmuth, J. Eckstein, B. Pfluger, Pfluger GHG-Neutral EU2050: Scenario of a European Union with Net-Zero Greenhouse Gas Emissions, 2019.
[10] Y. Zeng, P. Xu, W. Yang, H. Chu, W. Wang, W. Dong, M. Chen, H. Bai, P. Ma, Soy protein-based adhesive with superior bonding strength and water resistance by designing densely crosslinking networks, Eur. Polym. J. 142 (2021), https://doi.org/10.1016/j.eurpolymj.2020.110128.
[11] J. Zhang, X. Xi, J. Liang, A. Pizzi, G. Du, S. Deng, Tannin-based adhesive crosslinked by furfuryl alcohol-glyoxal and epoxy resins, Int. J. Adhesion Adhes. 94 (2019) 47–52, https://doi.org/10.1016/j.ijadhadh.2019.04.012.
[12] S. Zhao, H. Pang, Z. Li, Z. Wang, H. Kang, W. Zhang, S. Zhang, J. Li, L. Li, Polyurethane as high-functionality crosslinker for constructing thermally driven dual-crosslinking plant protein adhesion system with integrated strength and ductility, Chem. Eng. J. 422 (2021), https://doi.org/10.1016/j.cej.2021.130152.
[13] J. Chen, S. Shi, S.Q. Zhou, W. Li, Developments in bio-based soy protein adhesives: a review, Macromol. Mater. Eng. 307 (2022), https://doi.org/10.1002/mame.202200277.
[14] M. Dunky, Wood adhesives based on natural resources: a critical review: Part I. Protein-based adhesives, Rev. Adhes. Adhes. 8 (2020) 199–332, https://doi.org/10.7569/RAA.2020.097309.
[15] N.D.V. Raydan, L. Leroyer, B. Charrier, E. Robles, Recent advances on the development of protein-based adhesives for wood composite materials—a review, Molecules 26 (2021), https://doi.org/10.3390/molecules26247617.
[16] L. Lorenz, C.R. Frihart, J.M. Wescott, Analysis of soy flour/phenol-formaldehyde adhesives for bonding wood, Wood Adhes. 2005 (2005) 501–505.
[17] H. Lei, Z. Wu, M. Cao, G. Du, Study on the soy protein-based wood adhesive modified by hydroxymethyl phenol, Polymers 8 (2016), https://doi.org/10.3390/polym8070256.
[18] A. Shavandi, A. Ali, A new adhesive from waste wool protein hydrolysate, J. Environ. Chem. Eng. 6 (2018) 6700–6706, https://doi.org/10.1016/j.jece.2018.10.022.
[19] D. Gao, B. Fan, B. Zhang, Y. Mi, Y. Zhang, Z. Gao, Storage stability of polyamidoamine-epichlorohydrin resin and its effect on the properties of defatted soybean flour-based adhesives, Int. J. Adhesion Adhes. 91 (2019) 92–101, https://doi.org/10.1016/j.ijadhadh.2019.03.006.
[20] W. Hand, Defatted Soy Flour Substitution in Phenol Formaldehyde and Methylene Diphenyl Diisocyanate Wood Adhesives and Their Curing Kinetic Behavior, 2018.
[21] B. Liu, Z. Li, J. Zhang, M. Du, F. Fang, F. Chen, An environment-friendly wood adhesive using modified wheat gluten by isophorone diisocyanate, Ind. Crops Prod. 173 (2021), https://doi.org/10.1016/j.indcrop.2021.114125.
[22] Z. Zhu, E. Zhang, Y. Tu, M. Ye, N. Chen, An eco-friendly wood adhesive consisting of soybean protein and cardanol-based epoxy for wood based composites, Polymers 14 (2022), https://doi.org/10.3390/polym14142831.
[23] X. Hao, D. Bin Fan, Preparation and characterization of epoxy-crosslinked soy protein adhesive, J. Adhes. Sci. Technol. 32 (2018) 2682–2692, https://doi.org/10.1080/01694243.2018.1517488.
[24] S. Amirou, A. Pizzi, X. Xi, Wheat protein hydrolysates-resorcinol–aldehydes as potential cold setting adhesives, Eur. J. Wood Wood Prod. (2019) 453–463, https://doi.org/10.1007/s00107-019-01405-y.
[25] B. Zhang, J. Li, Y. Kan, J. Gao, Y. Zhang, Z. Gao, The effect of thermo-chemical treatment on the water resistance of defatted soybean flour-based wood adhesive, Polymers 10 (2018), https://doi.org/10.3390/polym10090955.
[26] P.L.H. McSweeney, P.F. Fox, Advanced dairy chemistry (2009), https://doi.org/10.1007/978-0-387-84865-5.
[27] B. Dukhnytskyi, World agricultural production, Ekon. APK (2019) 59–65, https://doi.org/10.32317/2221-1055.201907059.
[28] W. V Davis, C. Weber, S.R. Skorbiansky, Vegetables and Pulses Outlook : December 2022 Vegetable Prices Spike in 2022 Vegetable and Pulse Impacts — Weather Woes in 2022, 2023.
[29] R. Nitesh C, HimanshuVig, meat substitute market by product type (Tofu-Based, tempeh-based, TVP-based, seitan-based, quorn-based, and others), source (Soy-Based, wheat-based, mycoprotein, pea-based and others), and category (frozen, refrigerated, and shelf stable), Global Opportun (2022). Chapter 4.
[30] U. Deliverable, EUs Feather-Based Economy : the Challenges Ahead, 2022.
[31] K.S. Sikora, D.O. McPolin, A.M. Harte, Shear strength and durability testing of adhesive bonds in cross-laminated timber, J. Adhes. 92 (2016) 758–777, https://doi.org/10.1080/00218464.2015.1094391.
[32] S.Y. Mousavi, J. Huang, K. Li, Investigation of epoxy-based wood adhesives, J. Appl. Polym. Sci. 136 (2019) 1–7, https://doi.org/10.1002/app.47741.
[33] European Chemicals Agency, Regulatory strategy for flame retardants. https://doi.org/10.2823/854233, 2023.
[34] J. Alongi, F. Bosco, F. Carosio, A. Di Blasio, G. Malucelli, A new era for flame retardant materials? Mater. Today 17 (2014) 152–153, https://doi.org/10.1016/j.mattod.2014.04.005.
[35] C.R. Frihart, H. Satori, Soy flour dispersibility and performance as wood adhesive, J. Adhes. Sci. Technol. 27 (2013) 2043–2052, https://doi.org/10.1080/01694243.2012.696948.
[36] H. Lin, S. Gunasekaran, International Journal of Adhesion & Adhesives Cow Blood Adhesive : Characterization of Physicochemical and Adhesion Properties, vol. 30, 2010, pp. 139–144, https://doi.org/10.1016/j.ijadhadh.2009.10.003.
[37] Z. He, Bio-based Wood Adhesives, first ed., CRC Press, 2017 https://doi.org/10.1201/9781315369242.
[38] Z. Wu, H. Lei, G. Du, Disruption of soy-based adhesive treated by Ca(OH) 2 and NaOH, J. Adhes. Sci. Technol. 27 (2013) 2226–2232, https://doi.org/10.1080/01694243.2013.768140.
[39] S. Alvarez, N.D.V. Raydan, I. Svahn, E. Gontier, K. Rischka, B. Charrier, E. Robles, Assessment and characterization of duck feathers as potential source of biopolymers from an upcycling perspective, Sustain. Times 15 (15) (2023) 14201, https://doi.org/10.3390/SU151914201, 2023) 14201.
[40] U.K. Laemmli, Cleavage of structural proteins during the assembly of the head of bacteriophage T4, Nature 227 (1970) 680–685, https://doi.org/10.1038/227680a0.
[41] O. Accessories, Small Sample Adapter, I (n.d.).
[42] A. Barth, Infrared spectroscopy of proteins, Biochim. Biophys. Acta - Bioenerg. 1767 (2007) 1073–1101, https://doi.org/10.1016/j.bbabio.2007.06.004.
[43] P.I. Haris, F. Severcan, FTIR spectroscopic characterization of protein structure in aqueous and non-aqueous media, J. Mol. Catal. B Enzym. 7 (1999) 207–221, https://doi.org/10.1016/S1381-1177(99)00030-2.
[44] A. Barth, C. Zscherp, What vibrations tell us about proteins, Q. Rev. Biophys. 35 (2002) 369–430, https://doi.org/10.1017/S0033583502003815.
[45] R.W. Sarver, W.C. Krueger, Protein secondary structure from fourier transform infrared spectroscopy: a data base analysis, Anal. Biochem. 194 (1991) 89–100, https://doi.org/10.1016/0003-2697(91)90155-M.
[46] W.K. Surewicz, H.H. Mantsch, D. Chapman, Determination of protein secondary structure by fourier transform infrared spectroscopy: a critical assessment, Biochemistry 32 (1993) 389–394, https://doi.org/10.1021/bi00053a001.
[47] P. Yu, J.J. McKinnon, C.R. Christensen, D.A. Christensen, Using synchrotron-based FTIR microspectroscopy to reveal chemical features of feather protein secondary structure: comparison with other feed protein sources, J. Agric. Food Chem. 52 (2004) 7353–7361, https://doi.org/10.1021/jf0490955.
[48] N. Kuhar, S. Sil, T. Verma, S. Umapathy, Challenges in application of Raman spectroscopy to biology and materials (2018) 25888–25908, https://doi.org/10.1039/c8ra04491k.
[49] D. Yu, X. Zhang, W. Zou, H. Tang, F. Yang, L. Wang, W. Elfalleh, Raman spectroscopy analysis of the effect of electrolysis treatment on the structure of soy protein isolate, J. Food Meas. Char. (2020), https://doi.org/10.1007/s11694-020-00716-6.
[50] E.U.C.Y.L.I. Han, Raman Spectroscopy Determines Structural Changes Associated with Gelation Properties of Fish Proteins Recovered at Alkaline pH, 2006, pp. 2178–2187.
[51] S.C. Abrahams, The crystal and molecular structure of orthorhombic sulfur, Acta Crystallogr. 8 (1955) 661–671, https://doi.org/10.1107/s0365110x55002089.
[52] J. Itkonen, L. Ghemtio, D. Pellegrino, P.J. Jokela, H. Xhaard, M.G. Casteleijn, Analysis of Biologics Molecular Descriptors towards Predictive Modelling for Protein Drug Development Using Time-Gated Raman Spectroscopy, 2022.
[53] S.A. Oladepo, K. Xiong, Z. Hong, S.A. Asher, I.K. Lednev, NIH Public Access 112 (2013) 2604–2628, https://doi.org/10.1021/cr200198a.UV.
[54] S. Todorovic, M. Teixeira, Resonance Raman spectroscopy of Fe – S proteins and their redox properties, JBIC, J. Biol. Inorg. Chem. 23 (2018) 647–661, https://doi.org/10.1007/s00775-018-1533-0.

[55] L.B. Poole, Free Radical Biology and Medicine the basics of thiols and cysteines in redox biology and chemistry, Free Radic. Biol. Med. 80 (2015) 148–157, https://doi.org/10.1016/j.freeradbiomed.2014.11.013.
[56] C. Narayana, Raman Spectroscopy and MD Simulations, 2022.
[57] A.M. Woodin, Molecular size, shape and aggregation of soluble feather keratin, Biochem. J. 57 (1954) 99–109, https://doi.org/10.1042/bj0570099.
[58] A.J. Poole, J.S. Church, M.G. Huson, Environmentally sustainable fibers from regenerated protein, Biomacromolecules 10 (2009) 1–8, https://doi.org/10.1021/bm8010648.
[59] N. Eslahi, F. Dadashian, N.H. Nejad, An investigation on keratin extraction from wool and feather waste by enzymatic hydrolysis, Prep. Biochem. Biotechnol. 43 (2013) 624–648, https://doi.org/10.1080/10826068.2013.763826.
[60] A.O. Warsame, N. Michael, D.M. O'Sullivan, P. Tosi, Identification and quantification of major faba bean seed proteins, J. Agric. Food Chem. 68 (2020) 8535–8544, https://doi.org/10.1021/acs.jafc.0c02927.
[61] G.A. Denavi, P. Montero, N. Adriana, Structural and Functional Properties of Soy Protein Isolate and Cod Gelatin Blend Films, vol. 5, 1900, pp. 2094–2101.
[62] Q. Tang, Y.H. Roos, S. Miao, Plant protein versus dairy proteins: a pH-dependency investigation on their structure and functional properties, Foods 12 (2023), https://doi.org/10.3390/foods12020368.
[63] S. G, K. Philippi, D.R. Briggs, A. Gilles, J.K. Hamilton, Carbohydrate component casein in 7S protein fraction * of soybean by ikunori KOSHIYAMA noda institute for scientific Japan received carbohydrate components in the 7S protein from soybean casein fraction were found to be mannase and hexosamine, The former 30 (1966).
[64] S. Utsumi, J.E. Kinsella, Forces involved in soy protein gelation: effects of various reagents on the formation, hardness and solubility of heat-induced gels made from 7S, 11S, and soy isolate, J. Food Sci. 50 (1985) 1278–1282, https://doi.org/10.1111/j.1365-2621.1985.tb10461.x.
[65] G.H. Docena, R. Fernandez, F.G. Chirdo, C.A. Fossati, Identification of casein as the major allergenic and antigenic protein of cow's milk, Allergy Eur. J. Allergy Clin. Immunol. 51 (1996) 412–416, https://doi.org/10.1111/j.1398-9995.1996.tb04639.x.
[66] M. Corredig, D.G. Dalgleish, The mechanisms of the heat-induced interaction of whey proteins with casein micelles in milk, Int. Dairy J. 9 (1999) 233–236, https://doi.org/10.1016/S0958-6946(99)00066-7.
[67] S. Jovanovic, M. Barac, O. Macej, T. Vucic, C. Lacnjevac, SDS-PAGE analysis of soluble proteins in reconstituted milk exposed to different heat treatments, Sensors 7 (2007) 371–383, https://doi.org/10.3390/s7030371.
[68] M. Paulsson, P. Dejmek, Thermal denaturation of whey proteins in mixtures with caseins studied by differential scanning calorimetry, J. Dairy Sci. 73 (1990) 590–600, https://doi.org/10.3168/jds.S0022-0302(90)78707-3.
[69] M.M. Bacigalupe, A. He, Z. Escobar, Effects of rheology and viscosity of biobased adhesives on bonding performance, in: Z. He (Ed.), Bio-Based Wood Adhes. Prep. Charact. Testing., CRC Press, Boca Raton, Florida, 2017, pp. 293–309, https://doi.org/10.1201/9781315369242-14.
[70] L. Outcomes, S. Criteria, Higher chemistry : unit 1 – chemical changes and structure Part B – bonding , structure and properties lesson 7 – properties of bonding : Solubility and Viscosity, (n.d.) 1–9.
[71] J. Steinhaus, B. Hausnerova, T. Haenel, M. Großgarten, B. Möginger, Curing kinetics of visible light curing dental resin composites investigated by dielectric analysis (DEA), Dent. Mater. 30 (2014) 372–380, https://doi.org/10.1016/j.dental.2013.12.013.
[72] I. Stanley, Sandler, Chemical, Biochemical, and Engineering Thermodynamics, John Wiley & Sons, 2017.
[73] D. Barrick, Biomolecular Thermodynamics, first ed., CRC Press, 2017.
[74] R. Qing, S. Hao, E. Smorodina, D. Jin, A. Zalevsky, S. Zhang, Protein design: from the aspect of water solubility and stability, Chem. Rev. 122 (2022) 14085–14179, https://doi.org/10.1021/acs.chemrev.1c00757.
[75] R.A. Latour, Fundamental principles of the thermodynamics and kinetics of protein adsorption to material surfaces, Colloids Surf., B 191 (2020) 110992, https://doi.org/10.1016/j.colsurfb.2020.110992.
[76] Y. Liu, R. Guo, pH-dependent structures and properties of casein micelles, Biophys. Chem. 136 (2008) 67–73, https://doi.org/10.1016/j.bpc.2008.03.012.
[77] D.J. McMahon, R.J. Brown, Composition, structure, and integrity of casein micelles: a review, J. Dairy Sci. 67 (1984) 499–512, https://doi.org/10.3168/jds.S0022-0302(84)81332-6.
[78] M. Cheema, M.S. Mohan, S.R. Campagna, J.L. Jurat-Fuentes, F.M. Harte, The association of low-molecular-weight hydrophobic compounds with native casein micelles in bovine milk, J. Dairy Sci. 98 (2015) 5155–5163, https://doi.org/10.3168/jds.2015-9461.
[79] P. Müller-Buschbaum, R. Gebhardt, S.V. Roth, Z.E. Metwalli, W. Doster, Effect of calcium concentration on the structure of casein micelles in thin films, Biophys. J. 93 (2007) 960–968, https://doi.org/10.1529/biophysj.107.106385.
[80] F. Khosa, A. Khan, K. Nasir, W. Shuaib, M. Budoff, R. Blankstein, M.E. Clouse, Influence of image acquisition on radiation dose and image quality: full versus narrow phase window acquisition using 320 MDCT, Sci. World J. 2013 (2013), https://doi.org/10.1155/2013/731590.
[81] S. Moelbert, Correlation between sequence hydrophobicity and surface-exposure pattern of database proteins, Protein Sci. 13 (2004) 752–762, https://doi.org/10.1110/ps.03431704.
[82] J. Feng, L. Liu, Y. Zhang, Q. Wang, H. Liang, H. Wang, P. Song, Rethinking the pathway to sustainable fire retardants, Explorations 3 (2023), https://doi.org/10.1002/EXP.20220088.
[83] Y. Matsuura, M. Takehira, Y. Joti, K. Ogasahara, Thermodynamics of protein denaturation at temperatures over 100 ° C : CutA1 mutant proteins substituted with hydrophobic and charged residues, Nat. Publ. Gr. (2015) 1–9, https://doi.org/10.1038/srep15545.
[84] V.M.P. Puyana, E.C. Triviño, M.J. Rosado, A.R.I. Martínez, Pea protein - based bioplastics crosslinked with genipin : analysis of the crosslinking evolution, J. Polym. Environ. (2023), https://doi.org/10.1007/s10924-023-02973-0.
[85] T.T. Yimer, Valorisation of Waste Chicken Feathers : Production of High-Value Materials By, 2017.
[86] A. Mishra, D. Jung, N.K. Kim, D. Bhattacharyya, Influence of chicken feather fibre processing technique on mechanical and fire performances of flame-retardant polypropylene composites, Compos. Part A Appl. Sci. Manuf. 165 (2023) 107338, https://doi.org/10.1016/j.compositesa.2022.107338.
[87] S. Cai, C. Chen, H. Guo, S. Chen, Z. Zhou, Z. Guo, Fire resistance test of transformers filled with natural ester insulating liquid 2019 (2019) 1560–1564, https://doi.org/10.1049/joe.2018.8853.
[88] R. Das, S. Vupputuri, Q. Hu, Y. Chen, H. Colorado, Z. Guo, Z. Wang, Synthesis and characterization of anti-flammable vinyl ester resin nanocomposites with surface-functionalized nanotitania, ES Mater. Manuf. 8 (2020) 46–53, https://doi.org/10.30919/esmm5f709.
[89] R.M. Lopachin, T. Gavin, Thiolate sites, Relevance To Pathophysiological 50 (2017) 195–205, https://doi.org/10.3109/10715762.2015.1094184.REACTIONS.